



HAL
open science

The influence of water-saturation on the strength of volcanic rocks and the stability of lava domes

Michael Heap, Claire Harnett, Jamie Farquharson, Patrick Baud, Marina Rosas-Carbajal, Jean-Christophe Komorowski, Marie E.S. Violay, H. Albert Gilg, Thierry Reuschlé

► To cite this version:

Michael Heap, Claire Harnett, Jamie Farquharson, Patrick Baud, Marina Rosas-Carbajal, et al.. The influence of water-saturation on the strength of volcanic rocks and the stability of lava domes. *Journal of Volcanology and Geothermal Research*, 2023, 444, pp.107962. 10.1016/j.jvolgeores.2023.107962 . hal-04305488

HAL Id: hal-04305488

<https://hal.science/hal-04305488v1>

Submitted on 24 Nov 2023

HAL is a multi-disciplinary open access archive for the deposit and dissemination of scientific research documents, whether they are published or not. The documents may come from teaching and research institutions in France or abroad, or from public or private research centers.

L'archive ouverte pluridisciplinaire **HAL**, est destinée au dépôt et à la diffusion de documents scientifiques de niveau recherche, publiés ou non, émanant des établissements d'enseignement et de recherche français ou étrangers, des laboratoires publics ou privés.

1 The influence of water-saturation on the strength of volcanic rocks and
2 the stability of lava domes

3

4 **Michael J. Heap^{1,2*}, Claire Harnett^{3*}, Jamie Farquharson^{4,5}, Patrick Baud¹, Marina**
5 **Rosas-Carbajal⁶, Jean-Christophe Komorowski⁶, Marie E.S. Violay⁷, H. Albert Gilg⁸, and**
6 **Thierry Reuschlé¹**

7

8 ¹ *Université de Strasbourg, CNRS, Institut Terre et Environnement de Strasbourg, UMR 7063,*
9 *5 rue René Descartes, Strasbourg F-67084, France*

10 ² *Institut Universitaire de France (IUF), Paris, France*

11 ³ *School of Earth Sciences, University College Dublin, Dublin, Ireland*

12 ⁴ *Institute for Research Administration, Niigata University, Ikarashi 2-8050, Nishi-ku, Niigata*
13 *950-2181, Japan*

14 ⁵ *Research Institute for Natural Hazards and Disaster Recovery, Niigata University, Ikarashi*
15 *2-8050, Nishi-ku, Niigata 950-2181, Japan*

16 ⁶ *Université de Paris Cité, Institut de Physique du Globe de Paris, CNRS, F-75005 Paris,*
17 *France*

18 ⁷ *Laboratory of Experimental Rock Mechanics, Ecole Polytechnique Fédérale de Lausanne,*
19 *Lausanne, Switzerland*

20 ⁸ *TUM School of Engineering and Design, Technical University of Munich, Arcisstrasse 21,*
21 *80333 Munich, Germany*

22

23 *Corresponding authors: Michael Heap (heap@unistra.fr) and Claire Harnett
24 (claire.harnett@ucd.ie)

25

26 **Abstract**

27 The rocks forming a volcanic edifice or dome are typically saturated or partially-
28 saturated with water. However, most experiments aimed at better understanding the mechanical
29 behaviour of volcanic rocks have been performed on dry samples, and therefore most large-
30 scale models designed to explore volcano stability have used parameters representative for dry
31 rock. Here, we present a combined laboratory and modelling study in which we (1) quantified
32 the influence of water-saturation on the mechanical behaviour of variably altered dome rocks
33 from La Soufrière de Guadeloupe (Eastern Caribbean) and (2) used these new data to
34 investigate the influence of water on dome stability. Our laboratory data show that the ratio of
35 wet to dry uniaxial compressive strength (UCS) and Young's modulus are $\sim 0.30\text{--}0.95$ and
36 $\sim 0.10\text{--}1.00$, respectively. In other words, the dome rocks were all mechanically weaker when
37 water-saturated. Further, the ratio of wet to dry UCS decreased with increasing alteration (the
38 wt% of secondary minerals in the rocks). Micromechanical modelling suggests that the
39 observed water-weakening is the result of a decrease in fracture toughness (K_{IC}) in the presence
40 of water. The ratio of wet to dry K_{IC} also decreases with increasing alteration, explaining why
41 water-weakening increased as a function of alteration. To explore the influence of water-
42 saturation on lava dome stability, we numerically generated lava domes in Particle Flow Code
43 using the experimental data corresponding to unaltered and altered rock under dry conditions.
44 The strength of the dome-forming rocks was then reduced to values corresponding to wet
45 conditions. Our modelling shows that, although the stability of the unaltered dome was not
46 influenced by water-saturation, larger displacements were observed for the wet altered dome.
47 Additional simulations in which we modelled a buried alteration zone within an otherwise
48 unaltered dome showed that higher displacements were observed when the dome was water-
49 saturated. We conclude that (1) the water-saturation reduces the UCS and Young's modulus of
50 volcanic rock, (2) larger decreases in UCS in the presence of water are observed for altered

51 rocks, and (3) the stability of a dome can be compromised by the presence of water if the dome
52 is altered, or contains an altered zone. These conclusions highlight that the degree of alteration
53 and water-saturation should be mapped and monitored at active volcanoes worldwide, and that
54 large-scale models should use values for water-saturated rocks when appropriate.

55

56 **Highlights**

- 57 • Water-saturation reduces the strength of volcanic rocks.
- 58 • Strength reduction in the presence of water is higher for altered volcanic rocks.
- 59 • Strength reduction in the presence of water can be explained by a reduction in fracture
60 toughness.
- 61 • The stability of altered flanks and domes, or those containing altered zones, is
62 jeopardised by water-saturation.

63

64 **Keywords:** hydrothermal alteration; uniaxial compressive strength; Young's modulus; fracture
65 toughness; dome collapse

66

67 **1 Introduction**

68 The short- and long-term strength of rock is influenced not only by pore fluid pressures,
69 but also by the presence of water within the void space (e.g., Baud et al., 2000; Brantut et al.,
70 2013). Based on experiments and micromechanical analyses, reductions to the strength of rock
71 associated with the presence of water are thought to be the result of a decrease in specific
72 surface energy, friction coefficient, and fracture toughness (e.g., Baud et al., 2000; Noël et al.,
73 2021), the presence of clay minerals (e.g., Hawkins and McConnell, 1992; Heap et al., 2019),
74 adsorption pressures (e.g., Risnes et al., 2005), and/or an increase in the efficiency of sub-
75 critical crack growth (e.g., Atkinson, 1984; Kranz et al., 1982; Masuda, 2001; Brantut et al.,
76 2013; Tang et al., 2018).

77 Although water-weakening (the ratio of wet to dry strength) is reasonably well-
78 documented for sedimentary rocks such as sandstone (e.g., Rutter and Mainprice, 1978; Chest
79 and Logan, 1986; Hawkins and McConnell, 1992; Baud et al., 2000; Duda and Renner, 2013;
80 Wasantha and Ranjith, 2014; Baud et al., 2015; Heap et al., 2019; Noël et al., 2021), carbonate
81 rocks (e.g., Risnes et al., 2005; Baud et al., 2016; Nicolas et al., 2016; Castagna et al., 2018),
82 and gypsum (e.g., Caselle et al., 2022), few data exist for volcanic rocks. For example, the onset
83 of inelastic compaction in tuff from Alban Hills (Italy) was reduced by the presence of water
84 (Zhu et al., 2011). The uniaxial compressive strength of tuffs containing alunite (Heap et al.,
85 2015) and zeolites and clay minerals (Heap et al., 2018) was also lower in the presence of water.
86 Zhu et al. (2016) found that the compressive strength of a basalt from Mt Etna (Italy) was
87 reduced in the presence of water. Finally, the uniaxial compressive strength and Young's
88 modulus of lava from Mount Unzen (Japan) (Kendrick et al., 2021) and the uniaxial
89 compressive strength of lavas from Mt. Etna, Volvic (France), Kumamoto (Japan), and Volcán
90 de Colima (Mexico) and a block-and-ash flow from Mt. Meager (Canada) (Heap and Violay,
91 2021) were reduced when saturated with water. While wet to dry strength ratios in these lavas,

92 which were relatively unaltered, were typically on the order of ~ 0.9 , this ratio in tuffs can reach
93 ~ 0.2 when the tuffs are characterised by high zeolite and clay mineral contents (Heap and
94 Violay, 2021).

95 The importance of understanding the influence of water on the strength and mechanical
96 behaviour of volcanic rocks is threefold. First, volcanoes are often saturated or partially-
97 saturated and, in the case of subaerial, ocean-island, and coastal volcanoes, their saturation state
98 also varies as a function of space and time (Hurwitz et al., 2003; Join et al., 2005; Aizawa et
99 al., 2009; Delcamp et al., 2016). Volcanoes can be saturated, or partially-saturated, with
100 meteoric water (approximately 45% of the world's active volcanoes lie in the Tropics and are
101 therefore prone to intense periods of precipitation; Matthews et al., 2002), magmatic fluids,
102 and, in the case of submarine, ocean-island, and coastal volcanoes, seawater. Second, modelling
103 has shown that the mechanical properties of dome- and edifice-forming rock plays a first-order
104 role in dictating their stability and therefore the risk of collapse and associated hazards (Apuani
105 et al., 2005; Reid et al., 2001; Moon et al., 2009; Borselli et al., 2011; Schaefer et al., 2013;
106 Heap et al., 2021a, b; Harnett and Heap, 2021; Wallace et al., 2022; Mordensky et al., 2022;
107 Harnett et al., 2022; Carr et al., 2022; Heap et al., 2023a) and so, if water-saturation reduces
108 rock strength, it must also decrease dome and edifice stability. As a result, volcano stability
109 models should, where and when appropriate, use the mechanical properties for water-saturated
110 volcanic rocks. Third, the frequency of landslides and the failure and collapse of volcanic slopes
111 and domes increases following heavy rainfall (Kerle and van Wyk de Vries, 2001; Matthews et
112 al., 2002; Matthews and Barclay, 2004; Elsworth et al., 2004; Simmons et al., 2004; Taron et
113 al., 2007; Saucedo et al., 2008; Hicks et al., 2010; Vázquez et al., 2022), which will likely be
114 exacerbated by the increase in heavy rainfall expected given the current trend in global warming
115 (Farquharson and Amelung, 2022).

116 The paucity of laboratory data aimed at understanding water-weakening in volcanic
117 rocks therefore hinders our ability to accurately assess the stability of volcanic domes and
118 flanks. Further, not only does hydrothermal alteration, a very common process at active
119 volcanoes worldwide, influence the physical and mechanical properties of volcanic rocks (e.g.,
120 Frolova et al., 2014; Pola et al., 2014; Wyering et al., 2014; Mordensky et al., 2018; Coats et
121 al., 2018; Heap et al., 2021a, 2021b; Darmawan et al., 2022; Kanakiya et al., 2021, 2022;
122 Schaefer et al., 2023), but altered rocks can also contain the minerals (e.g., alunite and clay
123 minerals) that are thought to promote water-weakening in volcanic rocks, and so it is of
124 particular importance to assess the influence of hydrothermal alteration on water-weakening in
125 volcanic rocks. Indeed, a deadly debris avalanche at Casita volcano (Nicaragua) in 1998 was
126 thought to be the combined result of hydrothermal alteration and heavy rainfall (van Wyk de
127 Vries et al., 2000; Kerle and van Wyk de Vries, 2001; Kerle et al., 2003; Opfergelt et al., 2006),
128 and a landslide on the northeastern side of the dome at Soufrière de Guadeloupe (Eastern
129 Caribbean) that followed extreme rainfall exposed a collapse scar characterised by intensely
130 hydrothermally altered materials (Figure 1b).

131 Here, therefore, we present the results of (1) experiments designed to assess the
132 influence of water-saturation on the mechanical properties of variably-altered volcanic rocks
133 and (2) large-scale numerical modelling in Particle Flow Code (PFC), informed by the
134 experimental data, that investigates the influence of water on the stability of a volcanic dome.
135 For the purpose of this study, we will use La Soufrière de Guadeloupe as a case study.

136

137 **2 Case Study: La Soufrière de Guadeloupe (Eastern Caribbean)**

138 La Soufrière de Guadeloupe is an active andesitic stratovolcano located on the French
139 island of Guadeloupe in the Eastern Caribbean (Komorowski et al., 2005; Moretti et al., 2020;
140 Figure 1a). Volcanic unrest at La Soufrière de Guadeloupe has been steadily increasing in the

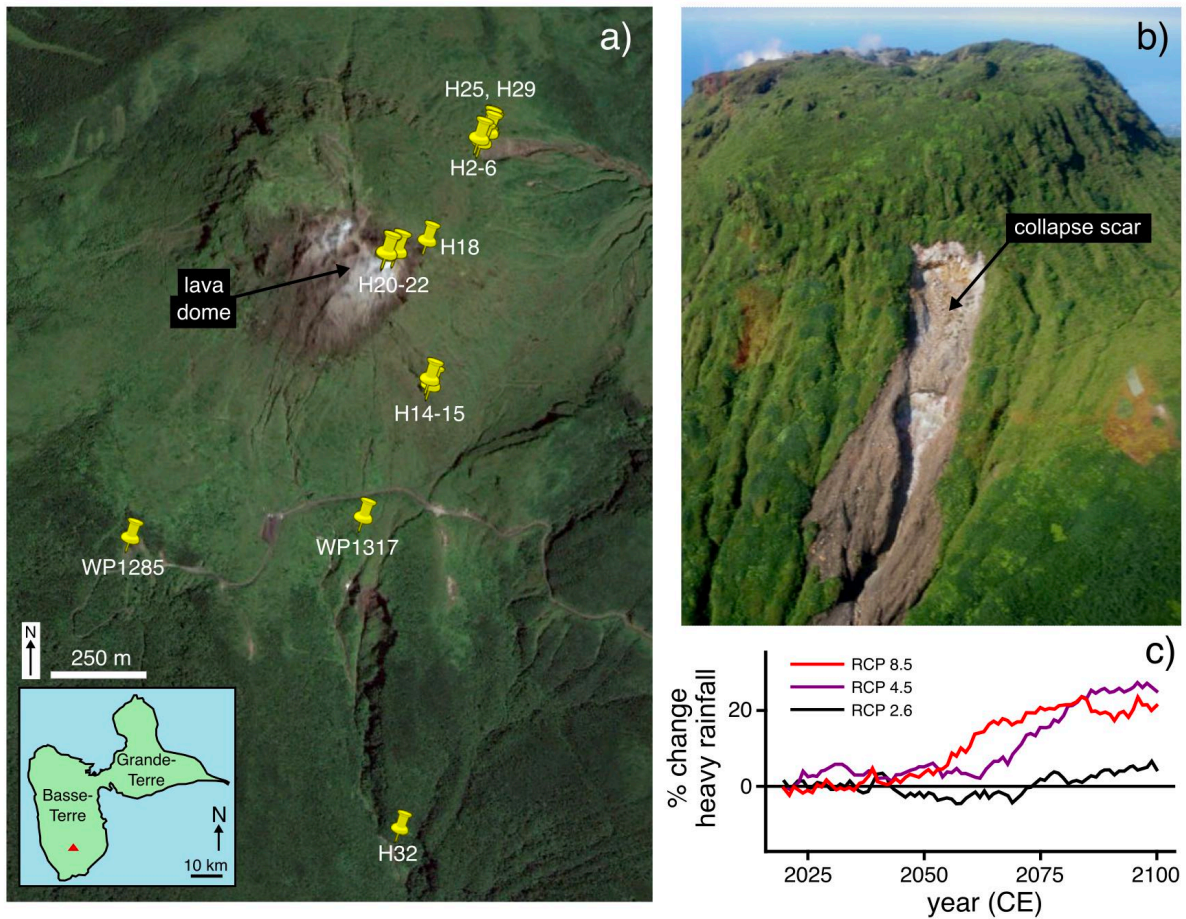
141 last three decades, manifest as an increase in the number of acid chloride-sulfate springs and
142 steam-dominated fumaroles, an increase in the heat output from the dome, an expansion of the
143 outgassing area at the top of the dome, an increase in flank and summit displacement rates, and
144 an abundance of shallow seismicity (including the largest felt tectonic earthquake since the last
145 eruption in 1976–1977, and frequent earthquake swarms that include several hundreds of
146 microearthquakes generated in few days and located within 1 km below the surface) (Brombach
147 et al., 2000; Villemant et al., 2005; Tamburello et al., 2019; Moretti et al., 2020; Heap et al.,
148 2021a; Jessop et al., 2021; Moune et al., 2022). Historically, partial edifice collapse has been
149 common at La Soufrière de Guadeloupe: at least nine flank collapses have occurred in the last
150 9150 years (Boudon et al., 2008; Komorowski et al., 2005; Legendre, 2012; Peruzzetto et al.,
151 2019), the most recent of which occurred in 1530 CE. Extensive hydrothermal alteration has
152 been identified as having a key role in these events, based on the abundance of altered materials
153 within the associated debris avalanche deposits (Komorowski et al., 2005; Le Friant et al., 2006;
154 Salaün et al., 2011; Rosas-Carbajal et al., 2016; Peruzzetto et al., 2019; Heap et al., 2021a). The
155 existence of hydrothermal fluid reservoirs (Brothelande et al., 2014; Rosas-Carbajal et al., 2016,
156 2017), perched aquifers (Lesparre et al., 2014), and the presence of listric-shaped, low-strength
157 layers formed by the superposition of flank-collapse slip surfaces within and below the La
158 Soufrière de Guadeloupe dome are anticipated to control the dynamics of future flank collapses
159 and other mass-wasting phenomena (Rosas-Carbajal et al., 2016; Peruzzetto et al., 2019).

160 Meteoric fluid input is also significant at La Soufrière de Guadeloupe; for example,
161 fumarole analysis by de Bremond d'Ars and Gibert (2022) highlights that meteoric input exerts
162 an importance control on the otherwise seemingly stochastic dynamics of the shallow
163 hydrothermal system. The volcano consistently receives over 5 m of rainfall annually at its
164 summit (Dessert et al., 2015), with as much as 30% of meteoric input infiltrating into the
165 groundwater (Rad et al., 2007). As a result, frequent smaller mass-wasting events at La

166 Soufrière de Guadeloupe have been directly related to intense rainfall events (Lesparre et al.,
167 2014), including landslides concurrent with the passage of storms and hurricanes (Allemand et
168 al., 2014); one such example is shown in Figure 1b. Very recently, parts of the *Chemin des*
169 *Dames*, a tourist path on the west flank of the dome, required repair following small-volume,
170 rain-induced landslides. This link between geohazards and the high-rainfall tropical climate
171 echoes a broader trend of rainfall-induced hazards observed at volcanoes elsewhere in the
172 Caribbean, including dome collapses (Matthews et al., 2002; Matthews and Barclay, 2004; Carn
173 et al., 2004) and seismicity (Matthews et al., 2009). In a comparative analysis of global climate
174 models, Farquharson and Amelung (2022) showed that models consistently project an increase
175 in heavy rainfall across the volcanic areas of the Caribbean over the next eight decades. In
176 Figure 1c, we plot projected change in heavy rainfall over La Soufrière de Guadeloupe obtained
177 from the MRI-CGCM3 general circulation model of Japan's Meteorological Research Institute:
178 clearly, the propensity for heavy rainfall events is set to increase in the near future (see also
179 Cantet et al., 2014), even under the most ambitious climate change mitigation strategies (i.e.
180 RCP 2.6).

181 Together, these factors highlight that La Soufrière de Guadeloupe represents an ideal
182 natural laboratory to study the influence of water-saturation on the physical and mechanical
183 properties of volcanic rock and volcano stability.

184



185

186

187

188

189

190

191

192

193

194

195

196

197

Figure 1. (a) Google Earth image (Google Maxar Technologies CNES / Airbus) of La Soufrière de Guadeloupe showing the sampling locations for the 17 rock blocks collected for this study. Inset shows a map of Guadeloupe in which the location of La Soufrière de Guadeloupe is indicated by a red triangle. (b) Photograph of the 2009 landslide scar on the northeastern flank of the dome (taken on 12 December 2009; photo credit: J.-B. de Chabalier, IPGP-OVSG). (c) Percentage change in heavy rainfall predicted for La Soufrière de Guadeloupe. Data are from the MRI-CGCM3 General Circulation Model results, provided by the Meteorological Research Institute, Japan, via the Earth System Grid Federation servers (<https://esgf-node.llnl.gov/search/cmip5/>). The change in projected heavy rainfall is resampled from monthly results corresponding to the 1.121×1.125 degree spatial grid containing La Soufrière de Guadeloupe, plotted as a function of time. For clarity, data are smoothed (15-year rolling mean) and normalised to 2023. Results are shown for three

198 separate future climate scenarios: a high emissions scenario (RCP 8.6), an intermediate
199 emissions scenario (RCP 4.5), and a "very stringent" pathway, whereby global carbon dioxide
200 emissions decrease to zero within 80 years (RCP 2.6). Further details are given in
201 Farquharson and Amelung (2022).

202

203 **3 Materials and Methods**

204 3.1 Experimental materials

205 A suite of 17 variably altered andesite blocks from La Soufrière de Guadeloupe were
206 used for this study (sampling locations are shown in Figure 1a). Eight of the 17 blocks were
207 collected from a collapse scar to the northeast of dome summit (blocks H2A, H2B, H3, H4A,
208 H5A, H6, H25, and H29). Four blocks were collected from the dome summit: one block from
209 the wall of the Lacroix Supérieur outgassing fracture on the lava dome (H18), and three blocks
210 from the lava spines that protrude the top of the current dome (one block from Cratère Sud
211 Central, H20, and two blocks from an adjacent site, H21 and H22). A block was collected to
212 the southwest of dome summit from a collapse scar into a highly fractured lava that forms the
213 core of a paleo-collapse mega-block of the former volcanic edifice (WP1285). Blocks were also
214 collected from the West wall of the fault "Faille du 30 août" on the lava dome (H14 and H15),
215 and from a thick lava adjacent to the Galion waterfall (H32). The final block is a volcanic non-
216 juvenile bomb from the dome that was ejected during the 1976–1977 explosive eruption
217 (Komorowski et al., 2005) and landed on the roof of a small disused thermal bathhouse to the
218 south of the dome summit (WP1317). We climbed on the roof of the bathhouse to collect the
219 block.

220 These 17 blocks, previously described by Heap et al. (2021a, 2022a, b, c, 2023a, b), are
221 porphyritic andesites characterised by a microcrystalline groundmass containing phenocrysts
222 of dominantly plagioclase and pyroxene (orthopyroxene and clinopyroxene). The mineral

223 assemblage present in each block was identified by a combination of optical microscopy,
 224 Raman spectroscopy, and X-ray powder diffraction (XRPD), and quantitative phase analysis
 225 was performed using the XRPD data and the Rietveld approach (for more details see Heap et
 226 al., 2021a). The XRPD data show that all of the rocks contain variable quantities of secondary
 227 (alteration) minerals: kaolinite, alunite or natro-alunite, silica polymorphs (quartz, cristobalite,
 228 tridymite, and opal-A), hematite, pyrite, gypsum, and talc (Heap et al. 2021a, 2022a, b, c; Table
 229 1). In this contribution, we quantify alteration as the wt% of secondary minerals in each block.
 230 The predominant hydrous alteration phases are kaolinite, natro-alunite, and opal-A (Table 1),
 231 suggesting fluid-rock interaction with acidic sulfate-chloride-rich fluids at relatively low
 232 temperatures (< 150–200 °C) (Inoue, 1995; Zimbelman et al., 2005; Scher et al., 2013;
 233 Fulignati, 2020; Heap et al., 2021a).

234

Mineral	H2A	H2B	H3	H4A	H5A	H6	H14	H15	H18	H20	H21	H22	H25	H29	H32	WP1285	WP1317
Plagioclase	56.7	12.3	46.6	23.3	41.3	30.0	60.7	22.5	61.2	28.7	24.2	59.5	38.7	62.4	64.4	64.7	61.6
Clinopyroxene	8.7	3.4	5.6	4.9	5.2	6.4	6.3	7.3	8.4	8.9	12.4	8.9	5.3	7.8	9.5	5.2	5.9
Orthopyroxene	10.8	9.5	11.8	11.8	11.1	10.8	8.6	9.2	12.2	15.0	19.3	13.6	10.2	11.2	15.1	13.2	15.6
(Ti-) Magnetite	0.7	-	0.8	-	-	-	0.8	-	2.9	2.4	3.1	0.8	-	2.7	4.9	3.5	0.7
Quartz*	1.0	0.5	0.6	0.6	0.5	0.5	1.7	0.7	0.7	0.3	0.2	0.6	0.3	0.4	0.3	0.2	0.7
Cristobalite*	11.3	12.8	10.6	11.8	13.0	11.1	13.5	10.2	11.7	11.4	11.7	10.6	9.8	12.4	5.7	-	-
Tridymite*	-	-	-	-	-	-	-	0.7	-	-	-	-	-	-	-	13.2	13.2
Hematite*	-	-	-	-	-	-	3.4	-	2.8	-	-	-	-	3.1	-	-	-
Pyrite*	3.5	-	3.8	2.3	-	-	-	-	-	-	0.4	3.1	0.6	-	-	-	-
Alunite*	-	-	-	-	-	-	-	-	-	-	-	-	-	-	-	-	2.4
Na-Alunite*	1.4	1.6	2.8	1.3	5.4	5.1	5.1	15.0	-	0.5	0.5	-	9.8	-	-	-	-
Gypsum*	-	-	-	0.7	-	-	-	-	-	0.8	1.2	-	-	-	-	-	-
Kaolinite*	6	59.7	17.4	43.3	23.5	36.0	< 1	34.3	-	2.0	2.0	< 1	25.3	-	-	-	-
Talc*	-	-	-	-	-	-	-	-	-	-	-	2.9	-	-	-	-	-
Opal-A*	-	-	-	-	-	-	-	-	-	30	25	-	-	-	-	-	-

235

236 **Table 1.** Mineral contents of the 17 rock blocks from La Soufrière de Guadeloupe measured
 237 by X-ray powder diffraction. Values in wt%. Asterisk denotes a secondary mineral (i.e.
 238 alteration mineral). Data from Heap et al. (2021a, 2022a, b, c). The relative uncertainties in
 239 the quantification are in the order of 5–10%. Sample locations are provided in Figure 1a.

240

241 3.2 Experimental methods

242 Cylindrical samples were prepared from each of the blocks to a diameter of 20 mm and
 243 then cut and precision-ground to a nominal length of 40 mm. The cylindrical samples cored

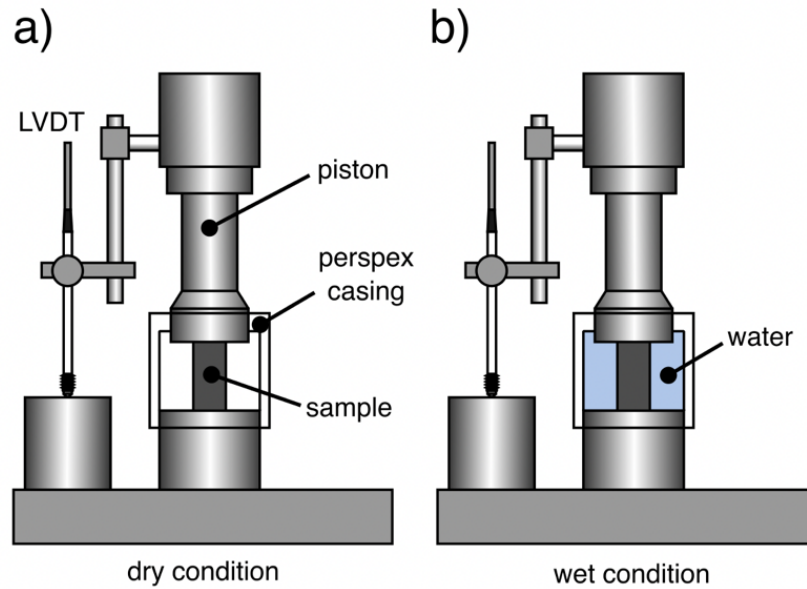
244 from a particular block were assumed to have the same mineral contents as the parent block
245 (i.e. those listed in Table 1). The samples were first washed using tapwater and then dried in a
246 vacuum-oven at 40 °C for at least 48 h. The connected porosity of all the samples was calculated
247 using the bulk sample volume and the skeletal (solid) sample volume of the oven-dry samples
248 measured by a helium pycnometer. Relative uncertainties of measurements of connected
249 porosity are < 2%.

250 Dry uniaxial compressive strength was measured on multiple oven-dry samples from
251 all 17 blocks in a uniaxial load frame located in the laboratory at the Strasbourg Institute of
252 Earth & Environment (ITES, France) (Figure 2a). Samples were deformed under ambient
253 laboratory pressure and temperature at a constant axial strain rate of 10^{-5} s^{-1} until macroscopic
254 failure. Axial displacement and axial load were measured using a linear variable differential
255 transducer and a load cell, respectively. Axial displacement (minus the displacement
256 accumulated within the load chain) and axial load were converted to axial strain and axial stress
257 using the sample dimensions. Relative uncertainties of measurements of uniaxial compressive
258 strength are < 1%. The static Young's modulus was determined from the elastic portion of the
259 uniaxial stress-strain curves (Heap et al., 2020a). Relative uncertainties of measurements of
260 Young's modulus are < 2%. The uniaxial compressive strength and Young's modulus of the
261 samples deformed dry were previously published in Heap et al. (2021a) (with the exception of
262 samples from block H32).

263 Water-saturated (wet) uniaxial compressive strength, data unique to this contribution,
264 was measured on multiple samples from all 17 blocks using the same uniaxial load frame, inside
265 a water bath (Figure 2b). The samples to be deformed under saturated conditions were
266 specifically selected so that their appearance and connected porosity was the same, or very
267 similar, to the samples deformed under dry conditions from the same block (so that their dry
268 and wet uniaxial compressive strength and Young's modulus can be compared directly). To do

269 so, multiple samples were prepared from each block and only those with a similar appearance
270 and porosity were selected for experimentation. Using this approach, the porosity difference
271 between each sample pair was in the range 0.00–0.03, which we consider to be sufficient to
272 allow for direct comparisons between the dry and wet uniaxial compressive strength and
273 Young's modulus of each of the blocks. Prior to deformation, the samples were vacuum-
274 saturated in de-aired, deionised water. The water-saturation procedure was as follows. (1) The
275 samples were placed inside a glass container, which was then placed within a bell jar. (2) The
276 samples were vacuumed inside the bell jar for at least 12 h at room temperature. (3) Maintaining
277 the vacuum inside the bell jar, de-aired, deionised water was introduced into the glass container
278 until the samples were completely submerged. (4) The samples were left submerged within the
279 vacuumed bell jar for at least 6 h, after which the vacuum was released and the glass container
280 containing the samples was removed from the bell jar. (5) The samples remained submerged in
281 de-aired, deionised water until deformed. As for the dry experiments, the static Young's
282 modulus was then determined from the elastic portion of the uniaxial stress-strain curves.
283 Samples from block H32, too strong to measure in the uniaxial load frame at the ITES, were
284 measured at the Laboratory of Experimental Rock Mechanics at the Ecole Polytechnique
285 Fédérale de Lausanne (EPFL, Switzerland) using a similar uniaxial setup. We consider the dry
286 samples deformed in Heap et al. (2021a) to have a water saturation of 0%, and the wet samples
287 deformed herein to have a water saturation of 100%.

288 Although rock strength and Young's modulus will increase as a function of pressure (or
289 depth) in the brittle regime, we highlight that lava domes are typically only a few hundred
290 metres high (the lava dome at La Soufrière de Guadeloupe, for example, is about 250–300 m
291 high) and that rock physical and mechanical properties (e.g., uniaxial compressive strength and
292 Young's modulus) will not change significantly under pressures representative of a depth of a
293 few hundred metres.



295

296 **Figure 2.** Schematic diagrams of the uniaxial compression apparatus at the Strasbourg
 297 Institute of Earth & Environment (ITES). (a) Setup for the dry experiments. (b) Setup for the
 298 wet experiments.

299

300 3.3 Numerical modelling

301 To explore the effect of water-saturation on dome stability, we used 2D Discrete
 302 Element Method (DEM) models created in Particle Flow Code (PFC; Itasca Consulting Group
 303 Ltd), following the methods outlined by Harnett et al. (2018) and Harnett and Heap (2021).
 304 PFC has been previously used to successfully model the mechanical behaviour of rock (e.g.,
 305 Potyondy and Cundall, 2004) and, recently, to model dome growth and collapse (Husain et al.,
 306 2014, 2018; Harnett et al., 2018; Husain et al., 2019; Harnett and Heap, 2021; Harnett et al.,
 307 2022; Walter et al., 2022; Heap et al., 2023a). These DEM models consider a particle-based
 308 material in which circular particles interact at interparticle contacts. Contact behaviour is
 309 primarily governed by stiffness and cohesion. At the boundary between the particles and walls
 310 (i.e. the ground surface), the contact behaviour is cohesionless and governed by friction. The

311 particle size in the model is not representative of individual crystals, grains, or rock blocks, but
312 rather represents discretisation of the medium for the purpose of computation.

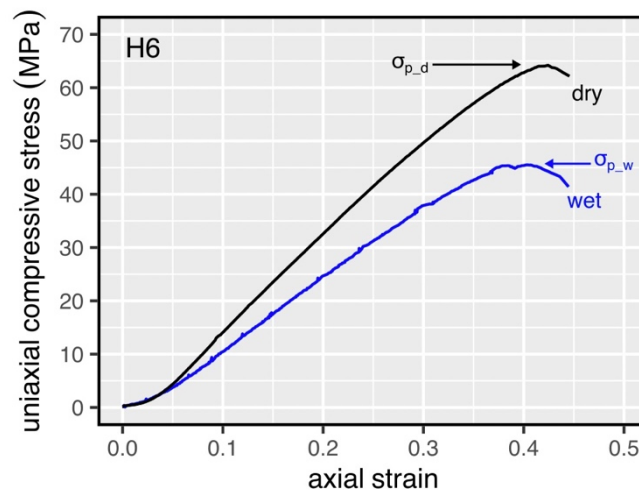
313 First, we numerically generated two fully solid domes (see Harnett and Heap, 2021)
314 containing 9745 circular particles and 22710 contacts. The contact properties were guided by
315 our experimental data for dry unaltered and altered dome rocks (uniaxial compressive strength,
316 tensile strength, and Young's modulus). An iterative calibration procedure was required to relate
317 contact parameters to bulk rock parameters, whereby uniaxial compression tests are reproduced
318 in PFC (see Harnett and Heap (2021) for details). Using these calibrated parameters, we created
319 initially stable dry unaltered and altered domes. These stable domes will not deform unless
320 perturbed in some way. To explore the effect of water-saturation on the stability of these domes,
321 we modified the mechanical properties of the contacts in the domes to represent wet unaltered
322 and altered dome rocks, also guided by our experimental data. The model then provided the
323 displacement within the dome resulting from water-saturation. Finally, we generated another
324 initially stable fully solid dome using properties representative of dry unaltered rock. In the first
325 scenario, we perturbed the dome by including a dry altered zone within the dome (as in Harnett
326 et al., 2022). In the second scenario, we also included the buried altered zone within the dome,
327 but, instead, we used properties representative of wet unaltered and altered rock. We highlight
328 that, although we use properties representative of uniaxial conditions in our models and,
329 therefore, we do not explicitly consider an increase in strength with depth in the model, the
330 models have an inherent depth-dependence of mechanical properties through the inclusion of
331 gravity: the contact forces at the base of the dome are much higher than those at the surface of
332 the dome. Further, as mentioned above, we also do not expect rock physical and mechanical
333 properties (e.g., uniaxial compressive strength and Young's modulus) to change significantly
334 under pressures representative of a depth of a few hundred metres. For the modelling of much
335 larger, or deeper, features, we recommend that triaxial deformation experiments are performed

336 to understand how rock physical and mechanical properties evolve as a function of pressure
337 (depth).

338

339 4 Results

340 Representative uniaxial stress-strain curves for dry and wet samples are shown in Figure
341 3 (for block H6). We highlight that the connected porosity of the dry and wet H6 samples shown
342 in Figure 3 is 0.18 and 0.16, respectively (Table 2). These curves show that the uniaxial
343 compressive strength and the Young's modulus (the slope of the stress-strain curve in the
344 pseudo-linear elastic regime) are lower when the sample is wet. We also note that the axial
345 strain at the peak stress is slightly lower for the wet sample than for the dry sample (Figure 3).
346



347

348 **Figure 3.** Representative stress-strain curves for dry (black curve) and wet (blue curve)
349 samples from block H6 from La Soufrière de Guadeloupe (Eastern Caribbean). The dry, $\sigma_{p,d}$,
350 and wet, $\sigma_{p,w}$, uniaxial compressive strengths are indicated on the curves.

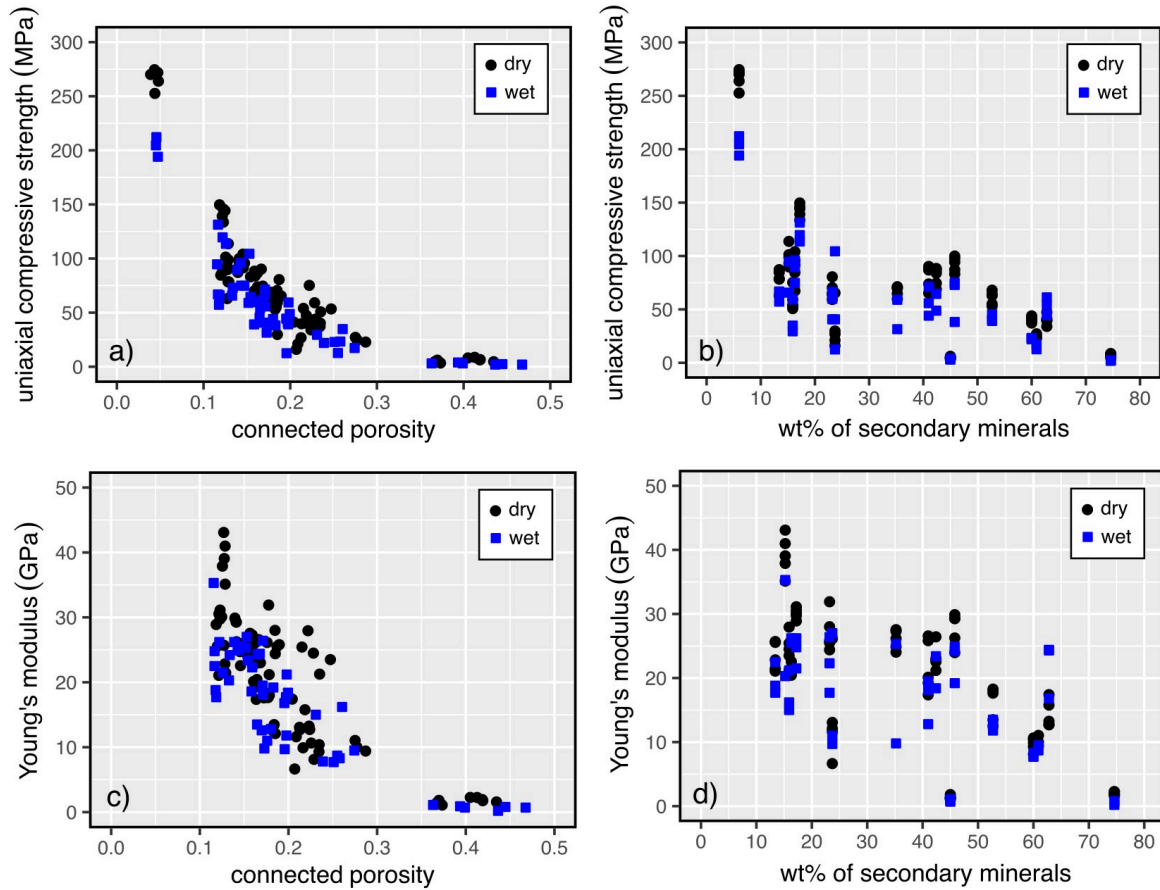
351

352 Dry (black circles) and wet (blue squares) uniaxial compressive strength data are plotted
353 as a function of connected porosity and the wt% of secondary minerals in Figures 4a and 4b,
354 respectively (data available in Table 2). These data show that uniaxial compressive strength

355 decreases as a function of connected porosity and the wt% of secondary minerals. For example,
356 strength decreased from ~270 MPa to only a couple of MPa as porosity decreased from ~0.05
357 to > 0.4 (Figure 4a). These data also show that, for a given porosity, the strength of wet samples
358 is typically lower than the strength of dry samples. Block H2B (porosity ~0.45; alteration 75
359 wt%; Table 2) and block H2A (porosity ~0.18; alteration 23 wt%) are characterised by the
360 lowest and highest ratio of wet to dry strength, respectively.

361 We also show dry (black circles) and wet (blue squares) Young's modulus as a function
362 of connected porosity and the wt% of secondary minerals in Figures 4c and 4d, respectively
363 (data available in Table 2). Similar to the strength data of Figure 4a and 4b, the data of Figure
364 4c and 4d show that (1) Young's modulus decreases as a function of connected porosity and
365 the wt% of secondary minerals and (2) for a given porosity, the Young's modulus of wet
366 samples is typically lower than the Young's modulus of dry samples. For example, Young's
367 modulus decreased from ~40 GPa to only a couple of GPa as porosity increases from ~0.05 to
368 > 0.4 (Figure 4c) or as the wt% of secondary minerals increases from ~15 to ~75 wt% (Figure
369 4d). Block H2B (porosity ~0.45; alteration 75 wt%; Table 2) and block WP1317 (porosity
370 ~0.14; alteration 16 wt%) are characterised by the lowest and highest ratio of wet to dry Young's
371 modulus, respectively.

372



373

374

Figure 4. Uniaxial compressive strength of dry (black circles) and wet (blue squares) samples

375

from La Soufrière de Guadeloupe (Eastern Caribbean) as a function of (a) connected porosity

376

and (b) the wt% of secondary minerals. Young's modulus of dry and wet samples from La

377

Soufrière de Guadeloupe as a function of (c) connected porosity and (d) the wt% of secondary

378

minerals. Dry data (apart from data for H32) are from Heap et al. (2021a). The relative

379

uncertainties of the connected porosity, uniaxial compressive strength, and Young's modulus

380

are $< 2\%$, $< 1\%$, and $< 2\%$, respectively; the uncertainties are therefore captured by the

381

symbol size. The relative uncertainties in the quantification of the mineral contents (Table 1)

382

are on the order of 5–10%.

383

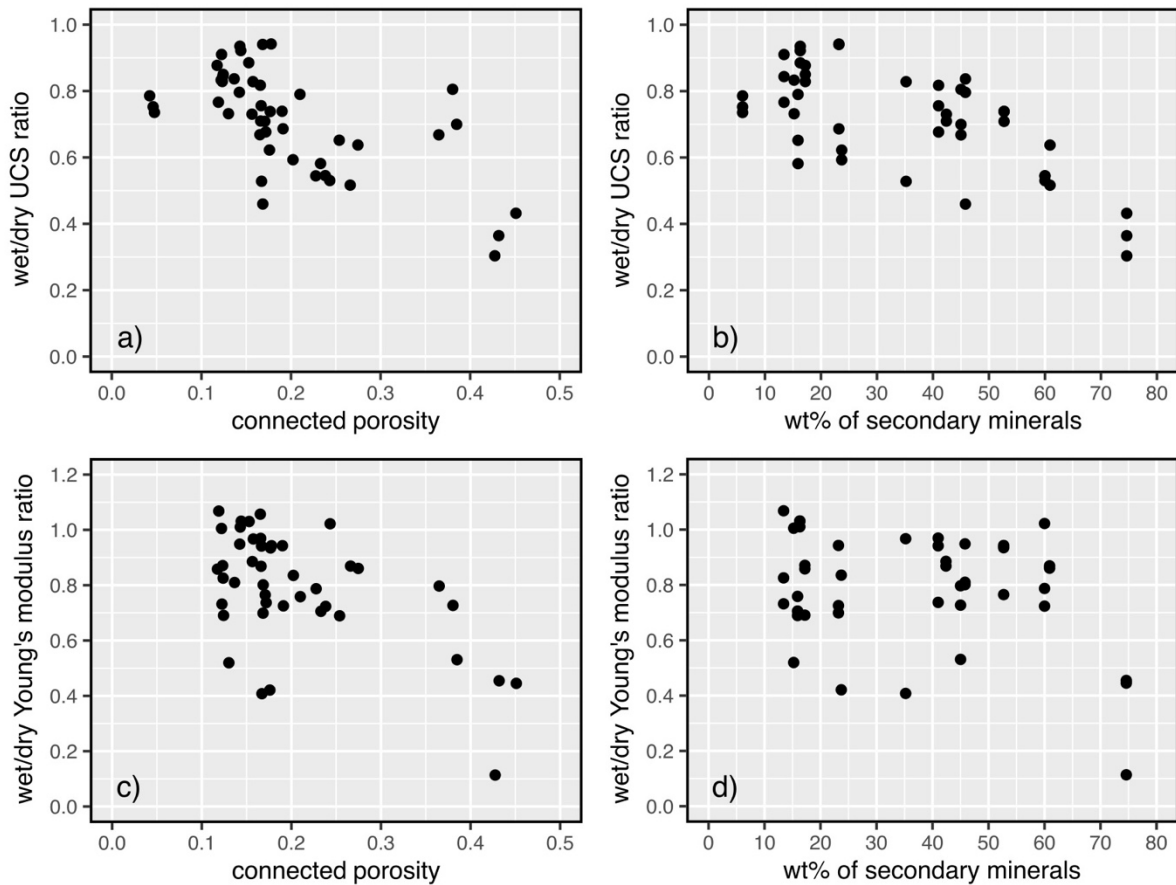
384

To better highlight the difference between wet and dry strength and Young's modulus,

385

the ratio of wet to dry strength and the ratio of wet to dry Young's modulus are plotted as a

386 function of connected porosity and the wt% of secondary minerals in Figure 5 (data available
387 in Table 3). This ratio is obtained by organising the samples from the same block deformed
388 under dry and wet conditions into pairs, and then dividing the data for the sample deformed
389 under saturated conditions with the data for their corresponding dry counterpart. As mentioned
390 above, the samples deformed under saturated conditions were specifically selected so that their
391 appearance and porosities were the same, or very similar, to those deformed under dry
392 conditions. A ratio of one therefore corresponds to the scenario in which the dry and wet
393 properties are exactly the same, and a ratio below and above one indicates that the sample
394 property is lower or higher when wet, respectively. Figure 5a shows that all of the samples have
395 a wet to dry strength lower than one, indicating that all samples were weaker when saturated
396 with water. These data also show that the wet to dry strength ratio appears to decrease as a
397 function of increasing porosity (Figure 5a) and wt% of secondary minerals (Figure 5b). Figure
398 5c shows that the majority of the samples have a wet to dry Young's modulus ratio below one.
399 Although the wet to dry Young's modulus ratio appears to decrease as a function of increasing
400 porosity (Figure 5c), there appears to be no discernible trend as a function of increasing wt%
401 of secondary minerals (Figure 5d), although we highlight that the samples with the lowest wet
402 to dry Young's modulus ratio contain the highest proportion of secondary minerals (Figure 5d).
403



404

405

406

407

408

409

410

411

412

413

Figure 5. Ratio of wet to dry uniaxial compressive strength (UCS) for samples from La Soufrière de Guadeloupe (Eastern Caribbean) as a function of (a) connected porosity and (b) the wt% of secondary minerals. Ratio of wet to dry Young's modulus for samples from La Soufrière de Guadeloupe as a function of (c) connected porosity and (d) the wt% of secondary minerals. The relative uncertainties of the connected porosity, uniaxial compressive strength, and Young's modulus are $< 2\%$, $< 1\%$, and $< 2\%$, respectively; the uncertainties are therefore captured by the symbol size. The relative uncertainties in the quantification of the mineral contents (Table 1) are on the order of 5–10%.

Sample	Weight percentage of secondary minerals	Connected porosity	Condition	Uniaxial compressive strength (MPa)	Young's modulus (GPa)
H2A 2	23	0.18	Dry	63.7	31.9
H2A 5	23	0.19	Dry	80.5	25.5
H2A 6	23	0.19	Dry	65.4	25.8

H2A 11	23	0.19	Dry	59.3	24.4
H2A 12	23	0.18	Dry	70.4	28.0
H2A 7	23	0.17	Wet	66.3	26.4
H2A 10	23	0.16	Wet	59.9	22.3
H2A 14	23	0.20	Wet	40.7	17.7
H2B 3	75	0.42	Dry	6.6	1.8
H2B 10	75	0.42	Dry	6.4	1.9
H2B 11	75	0.41	Dry	8.7	2.3
H2B 12	75	0.41	Dry	8.1	2.3
H2B 15	75	0.43	Dry	4.6	1.6
H2B 7	75	0.44	Wet	2.0	0.2
H2B 9	75	0.47	Wet	2.0	0.7
H2B 13	75	0.44	Wet	2.4	0.8
H3 3	35	0.16	Dry	70.3	27.3
H3 7	35	0.16	Dry	69.9	24.9
H3 8	35	0.16	Dry	64.8	27.5
H3 11	35	0.16	Dry	59.7	24.0
H3 13	35	0.16	Dry	71.2	26.2
H3 14	35	0.17	Wet	31.5	9.8
H3 15	35	0.15	Wet	59.0	25.3
H4A 2	60	0.23	Dry	40.3	10.4
H4A 4	60	0.23	Dry	42.0	10.6
H4A 6	60	0.23	Dry	43.9	8.1
H4A 8	60	0.23	Dry	37.2	9.3
H4A 9	60	0.22	Dry	40.4	9.9
H4A 5	60	0.25	Wet	22.9	.77
H4A 7	60	0.26	Wet	23.3	8.3
H4A 10	60	0.24	Wet	22.0	7.8
H5A 2	42	0.16	Dry	88.3	26.4
H5A 3	42	0.16	Dry	86.6	22.8
H5A 5	42	0.16	Dry	83.9	22.5
H5A 8	42	0.18	Dry	68.8	21.2
H5A 10	42	0.17	Dry	74.5	23.0
H5A 4	42	0.20	Wet	48.8	18.4
H5A 9	42	0.15	Wet	64.5	23.4
H6 6	53	0.18	Dry	55.1	13.5
H6 9	53	0.18	Dry	68.0	18.0
H6 9	53	0.18	Dry	53.0	12.5
H6 12	53	0.18	Dry	64.2	17.6
H6 13	53	0.18	Dry	63.0	18.3
H6 2	53	0.16	Wet	45.5	13.5
H6 3	53	0.20	Wet	39.2	11.8
H6 5	53	0.17	Wet	40.7	12.6
H14 2	24	0.18	Dry	65.4	26.1
H14 3	24	0.21	Dry	21.1	11.6
H14 5	24	0.21	Dry	26.8	13.1
H14 6	24	0.19	Dry	29.8	12.1
H14 10	24	0.21	Dry	16.1	6.6
H14 8	24	0.20	Wet	12.5	9.7
H14 11	24	0.18	Wet	40.7	11.0
H15 3	61	0.28	Dry	24.6	10.0
H15 4	61	0.28	Dry	27.1	11.0
H15 5	61	0.29	Dry	22.8	9.4
H15 6	61	0.27	Wet	17.3	9.5
H15 7	61	0.25	Wet	12.7	8.7
H18 3	15	0.13	Dry	101.3	37.9
H18 4	15	0.13	Dry	89.8	39.1
H18 5	15	0.13	Dry	98.8	41.0

H18 6	15	0.13	Dry	93.2	43.1
H18 7	15	0.13	Dry	113.7	35.1
H18 11	15	0.13	Wet	65.7	20.3
H18 14	15	0.12	Wet	94.7	35.3
H20 2	45	0.37	Dry	4.8	1.2
H20 3	45	0.37	Dry	4.4	1.3
H20 7	45	0.37	Dry	4.6	1.4
H20 8	45	0.37	Dry	6.1	1.8
H20 10	45	0.37	Dry	3.4	1.1
H20 5	45	0.39	Wet	3.9	0.9
H20 6	45	0.40	Wet	3.1	0.7
H20 11	45	0.36	Wet	3.1	1.1
H21 3	41	0.17	Dry	90.2	26.6
H21 8	41	0.16	Dry	65.2	17.4
H21 11	41	0.16	Dry	86.9	25.8
H21 12	41	0.16	Dry	73.8	19.2
H21 13	41	0.16	Dry	87.2	20.1
H21 4	41	0.17	Wet	71.3	19.5
H21 6	41	0.18	Wet	44.1	12.8
H21 15	41	0.17	Wet	55.8	18.1
H22 2	17	0.12	Dry	145.7	29.7
H22 3	17	0.12	Dry	144.3	30.1
H22 4	17	0.12	Dry	139.1	30.5
H22 5	17	0.12	Dry	149.7	28.9
H22 6	17	0.12	Dry	133.6	31.1
H22 7	17	0.12	Wet	119.6	26.2
H22 14	17	0.12	Wet	131.3	24.8
H22 15	17	0.13	Wet	113.6	21.5
H25 2	46	0.14	Dry	99.9	29.3
H25 4	46	0.14	Dry	97.7	29.3
H25 5	46	0.14	Dry	94.2	26.2
H25 9	46	0.14	Dry	87.1	29.9
H25 12	46	0.15	Dry	83.1	24.0
H25 3	46	0.18	Wet	38.2	19.2
H25 10	46	0.13	Wet	72.9	24.2
H25 14	46	0.14	Wet	75.0	24.9
H29 2	16	0.22	Dry	53.9	25.4
H29 8	16	0.23	Dry	59.1	24.5
H29 9	16	0.22	Dry	75.2	27.9
H29 12	16	0.25	Dry	53.4	23.5
H29 16	16	0.24	Dry	50.7	21.3
H29 3	16	0.20	Wet	59.4	21.2
H29 6	16	0.26	Wet	34.8	24.2
H29 13	16	0.23	Wet	29.5	24.9
H32 1	6	0.04	Dry	270.1	-
H32 4	6	0.05	Dry	263.9	-
H32 5	6	0.05	Dry	271.9	-
H32 6	6	0.04	Dry	274.5	-
H32 7	6	0.04	Dry	252.6	-
H32 8	6	0.05	Wet	194.1	-
H32 9	6	0.05	Wet	204.6	-
H32 10	6	0.04	Wet	212.2	-
WP1285 2	13	0.13	Dry	78.5	22.8
WP1285 8	13	0.13	Dry	63.0	25.7
WP1285 10	13	0.13	Dry	78.3	21.4
WP1285 11	13	0.12	Dry	87.2	21.1
WP1285 15	13	0.12	Dry	84.6	25.6
WP1285 4	13	0.12	Wet	66.1	17.7

WP1285_6	13	0.12	Wet	57.3	18.8
WP1285_9	13	0.12	Wet	66.8	22.5
WP1317_2	16	0.16	Dry	67.3	20.4
WP1317_6	16	0.16	Dry	84.5	24.7
WP1317_7	16	0.15	Dry	91.5	22.6
WP1317_8	16	0.15	Dry	95.8	25.9
WP1317_12	16	0.15	Dry	104.0	24.7
WP1317_10	16	0.15	Wet	74.8	25.5
WP1317_13	16	0.14	Wet	89.6	26.2
WP1317_15	16	0.14	Wet	95.9	25.5

414

415 **Table 2.** Experimental condition (dry or wet), connected porosity, uniaxial compressive
416 strength, Young's modulus, and the percentage of secondary minerals (i.e. alteration) for the
417 samples prepared for this study. Sample locations are provided in Figure 1a. Dry data (apart
418 from data for H32) are from Heap et al. (2021a). The relative uncertainties of the connected
419 porosity, uniaxial compressive strength, and Young's modulus are < 2%, < 1%, and < 2%,
420 respectively. The relative uncertainties in the quantification of the mineral contents (Table 1)
421 are on the order of 5–10%.

422

Sample	Weight percentage of secondary minerals	Connected porosity	wet/dry UCS ratio	wet/dry Young's modulus ratio
H2A	23	0.17	0.94	0.70
H2A	23	0.18	0.94	0.94
H2A	23	0.19	0.69	0.73
H2B	75	0.45	0.43	0.45
H2B	75	0.43	0.30	0.11
H2B	75	0.43	0.36	0.45
H3	35	0.17	0.53	0.41
H3	35	0.16	0.83	0.97
H4A	60	0.23	0.54	0.79
H4A	60	0.24	0.55	0.72
H4A	60	0.24	0.53	1.02
H5A	42	0.16	0.73	0.89
H5A	42	0.17	0.71	0.87
H6	53	0.17	0.71	0.77
H6	53	0.19	0.74	0.94
H6	53	0.18	0.74	0.93
H14	24	0.20	0.59	0.84
H14	24	0.18	0.62	0.42
H15	61	0.27	0.64	0.86
H15	61	0.27	0.52	0.87
H18	15	0.12	0.83	1.01
H18	15	0.13	0.73	0.52
H20	45	0.38	0.81	0.73

H20	45	0.38	0.70	0.53
H20	45	0.36	0.67	0.80
H21	41	0.17	0.82	0.97
H21	41	0.17	0.68	0.74
H21	41	0.17	0.76	0.94
H22	17	0.12	0.85	0.69
H22	17	0.12	0.88	0.86
H22	17	0.12	0.83	0.87
H25	46	0.14	0.80	0.95
H25	46	0.14	0.84	0.81
H25	46	0.17	0.46	0.80
H29	16	0.21	0.79	0.76
H29	16	0.25	0.65	0.69
H29	16	0.23	0.58	0.71
H32	6	0.05	0.74	-
H32	6	0.05	0.75	-
H32	6	0.04	0.79	-
WP1285	13	0.12	0.77	1.07
WP1285	13	0.12	0.91	0.73
WP1285	13	0.12	0.84	0.83
WP1317	16	0.14	0.92	1.03
WP1317	16	0.14	0.93	1.01
WP1317	16	0.15	0.89	1.03

423

424 **Table 3.** Percentage of secondary minerals (i.e. alteration), average connected porosity, the
425 ratio of wet to dry uniaxial compressive strength, and the ratio of wet to dry Young's modulus
426 for the samples prepared for this study. Sample locations are provided in Figure 1a. The
427 relative uncertainties of the connected porosity, uniaxial compressive strength, and Young's
428 modulus are < 2%, < 1%, and < 2%, respectively. The relative uncertainties in the
429 quantification of the mineral contents (Table 1) are on the order of 5–10%.

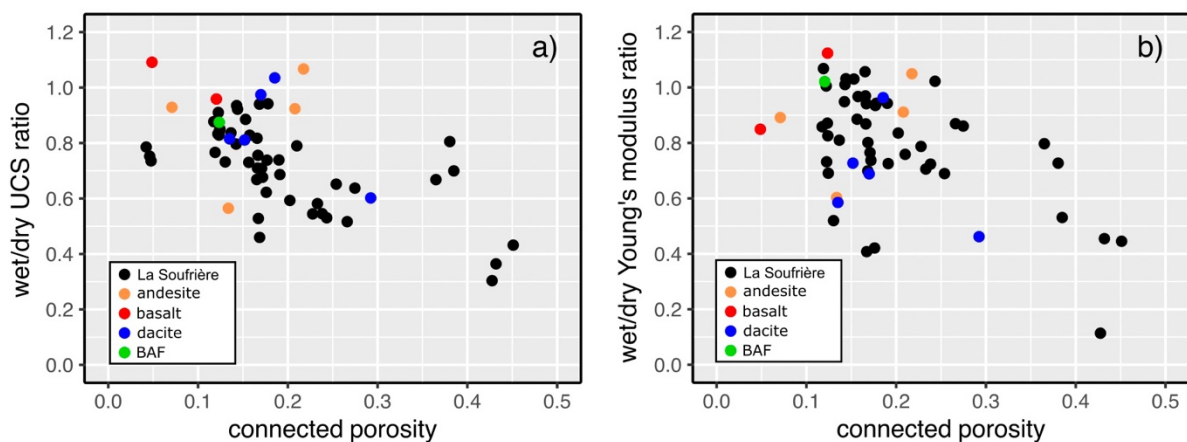
430

431 **5 Discussion**

432 5.1 Water-weakening in volcanic rocks: the influence of porosity

433 Our data show that the uniaxial compressive strength and Young's modulus of variably-
434 altered dome lavas from La Soufrière de Guadeloupe are reduced when water-saturated
435 (Figures 4 and 5), in agreement with previous studies on volcanic rocks (Zhu et al., 2011; Heap
436 et al., 2015; Zhu et al., 2016; Heap et al., 2018; Kendrick et al., 2021; Heap and Violay, 2021).

437 We plot the ratio of wet to dry strength and the ratio of wet to dry Young's modulus as
438 a function of connected porosity for our new data alongside published data for volcanic rocks
439 in Figures 6a and 6b, respectively. Figures 6a and 6b show that, based on previously published
440 data for andesite, basalt, dacite, and welded block-and-ash flow, one would conclude that water-
441 weakening in volcanic rocks does not appear to vary systematically with porosity. Previous
442 studies have also shown that porosity does not appear to influence water-weakening in
443 sandstones (Heap et al., 2019), limestones (Baud et al., 2016), and tuffs (Zhu et al., 2011; Heap
444 et al., 2018; Frolova et al., 2021). Our new data for hydrothermally altered andesites from La
445 Soufrière de Guadeloupe, however, suggest that porosity exerts influence on their water-
446 weakening behaviour (Figures 6a and 6b). This may be because the porosity range studied in
447 previous contributions was insufficient to observe a trend (the most porous sample from the
448 previously published dataset is a dacite with a porosity of ~ 0.3 , whereas the maximum porosity
449 in our dataset is ~ 0.45 ; Figures 6 and 6b). Although we conclude that porosity appears to exert
450 influence on water-weaking in our sample suite, we suggest that more data for high-porosity
451 volcanic rocks are now required to make firm conclusions as to the influence of porosity on
452 water-weakening in volcanic rocks (based on reasoning discussed in the next subsection).
453



454

455 **Figure 6.** Ratio of wet to dry (a) uniaxial compressive strength and (b) Young's
456 modulus for samples from La Soufrière de Guadeloupe (Eastern Caribbean) as a function of
457 connected porosity (black circles). Data for andesite (orange circles), basalt (red circles), and
458 block-and-ash flow (BAF; green circles) from Heap and Violay (2021). Data for dacite (blue
459 circles) from Kendrick et al. (2021). For the data for the samples from La Soufrière de
460 Guadeloupe, the relative uncertainties of the connected porosity, uniaxial compressive
461 strength, and Young's modulus are $< 2\%$, $< 1\%$, and $< 2\%$, respectively; the uncertainties are
462 therefore captured by the symbol size.

463

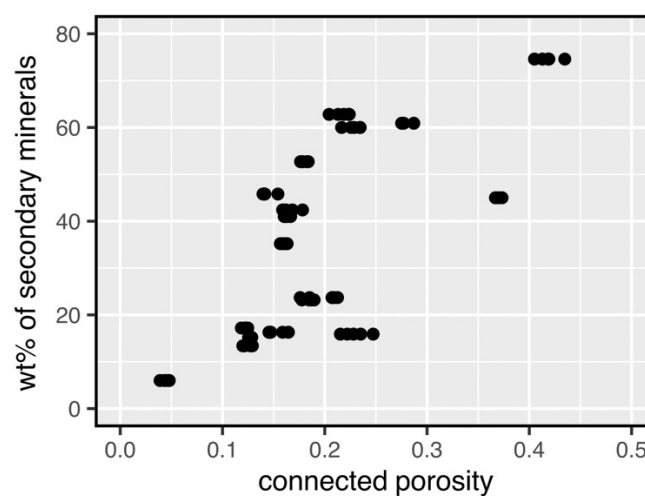
464 5.2 Water-weakening in volcanic rocks: the influence of alteration

465 We first note that the uniaxial compressive strength (Figure 4b) and Young's modulus
466 (Figure 4d) of water-saturated andesites from La Soufrière de Guadeloupe are reduced as a
467 function of increasing wt% of secondary minerals. Previously, hydrothermal alteration has been
468 shown to either decrease (e.g., Frolova et al., 2014; Pola et al., 2014; Wyering et al., 2014;
469 Mordensky et al., 2018, 2019; Heap et al., 2021a; Darmawan et al., 2022; Schaefer et al., 2023)
470 or increase the strength of volcanic rocks (e.g., Frolova et al., 2014; Pola et al., 2014; Wyering
471 et al., 2014; Coats et al., 2018; Heap et al., 2020b, 2021b). These studies, and others, have
472 shown that whether or not hydrothermal alteration decreases or increases strength depends on
473 the type of alteration and/or whether the alteration results in increases or decreases to porosity.

474 In the case of hydrothermally altered dome rocks from La Soufrière de Guadeloupe,
475 Heap et al. (2021a, 2022) concluded that alteration had reduced their uniaxial compressive
476 strength and Young's modulus. However, these authors also noted that there is a relationship
477 between porosity and alteration (Figure 7). As discussed by these authors, it is difficult to
478 unravel the influence of porosity and alteration on the strength of these materials because it is
479 unclear whether alteration increased the porosity of the samples or whether the more porous

480 samples are more altered due to their higher fluid-rock ratios. However, based on the presence
481 of abundant clays and dissolution textures in these samples, Heap et al. (2021a, 2022) concluded
482 uniaxial compressive strength and Young's modulus were likely reduced by hydrothermal
483 alteration. We conclude the same here, although we highlight that the main focus of this
484 contribution is to study the influence of water-saturation on the mechanical properties of
485 hydrothermally altered dome rocks, discussed below.

486



487

488 **Figure 7.** The wt% of secondary minerals as a function of connected porosity for samples
489 from La Soufrière de Guadeloupe (Eastern Caribbean).

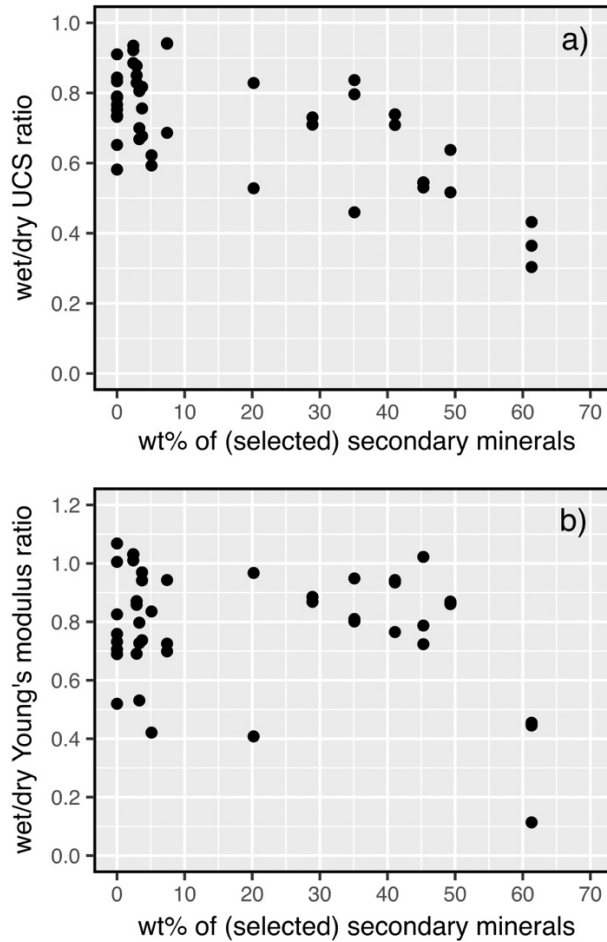
490

491 Our data suggest that the wet to dry strength ratio decreases as a function of increasing
492 wt% of secondary minerals (Figure 5b), although there appears to be no discernible trend in the
493 wet to dry Young's modulus ratio as a function of increasing wt% of secondary minerals (Figure
494 5d). In other words, these data suggest that the reduction in strength due to the presence of water
495 increases as a function of the degree of hydrothermal alteration and, therefore, the abundance
496 of secondary (alteration) minerals. These results are in agreement with the previous laboratory
497 data for tuff, which suggest that the presence of alunite (Heap et al., 2015) and zeolites and clay
498 minerals (Heap et al., 2018) may be responsible for the reduction in uniaxial compressive

499 strength in the presence of water. Expansive clay minerals, for example, can mechanically
500 degrade as a function of increasing water content (Nara et al., 2012). The fact that alteration
501 increases the observed water-weakening (Figure 5b) and that alteration increases as a function
502 of connected porosity for these rocks (Figure 7) also suggests that the observed trends as a
503 function of porosity (Figures 6a and 6b) could be because the high-porosity rocks are more
504 altered, and it is the alteration that is dictating the observed water-weakening. As stated above,
505 more experiments are now required to make firm conclusions as to the influence of porosity on
506 water-weakening in volcanic rocks.

507 To further investigate the influence of alteration on water-weakening, we replot the ratio
508 of wet to dry uniaxial compressive strength and Young's modulus as a function of a subset of
509 the alteration minerals (alunite, Na-alunite, gypsum, kaolinite, and talc only; i.e. excluding
510 cristobalite, tridymite, hematite, pyrite, and opal-A) in Figure 8. We include those minerals that
511 have previously been considered to reduce the strength of rock upon water-saturation. We
512 highlight that the coefficients of determination for simple linear fits to the data shown in Figure
513 8 are very similar to those for the data shown in Figures 5b and 5d. Therefore, these data suggest
514 that the selected alteration minerals (alunite, Na-alunite, gypsum, kaolinite, and talc) are likely
515 those influencing the uniaxial compressive strength of these rocks in the presence of water
516 (Figure 8a).

517



518

519 **Figure 8.** Ratio of wet to dry (a) uniaxial compressive strength and (b) Young's modulus as a
 520 function of the wt% of a subset of the secondary minerals for samples from La Soufrière de
 521 Guadeloupe (Eastern Caribbean). The alteration minerals included are alunite, Na-alunite,
 522 gypsum, kaolinite, and talc only (i.e. excluding cristobalite, tridymite, hematite, pyrite, and
 523 opal-A). The relative uncertainties of the uniaxial compressive strength and Young's modulus
 524 are $< 1\%$ and $< 2\%$, respectively; the uncertainties are therefore captured by the symbol size.

525 The relative uncertainties in the quantification of the mineral contents (Table 1) are on the
 526 order of 5–10%.

527

528 To investigate the mechanism responsible for the observed weakening in the presence
 529 of water, and the increase in water-weakening as a function of alteration (Figures 4b, 5b, and

530 8a), we use the analytical approximation of Sammis and Ashby's (1986) pore-emanating crack
531 micromechanical model provided by Zhu et al. (2010):

532

$$533 \quad UCS = \frac{1.325 K_{IC}}{\phi^{0.414} \sqrt{\pi r}} \quad (1).$$

534

535 The pore-emanating crack model of Sammis and Ashby (1986) has been widely used to
536 investigate the mechanical behaviour of porous volcanic rocks (see Heap and Violay (2021) for
537 a review). The pore-crack model describes a two-dimensional elastic medium populated with
538 circular pores of a uniform radius. In the model, cracks can propagate in a direction parallel to
539 the maximum principal stress when the stress at the tip of a crack on the curved surface of the
540 pore reaches the fracture toughness of the material, K_{IC} (the resistance of a brittle material to
541 the propagation of cracks under an applied stress). Eventually, the cracks grow long enough to
542 interact and ultimately coalesce, resulting in the macroscopic failure of the medium. Although
543 the andesites studied here contain microcracks, their microstructure can be well approximated
544 by this inclusion model (i.e. pores within a groundmass; Heap et al., 2021a), although we
545 highlight that the model assumes a uniform pore radius. In the analytical solution to the model
546 (Equation (1)), uniaxial compressive strength (UCS) is a function of K_{IC} , porosity, ϕ , and pore
547 radius, r . The two unknowns in Equation (1) are K_{IC} and r . We can estimate r using
548 microstructural analysis. To do so, we calculated the average equivalent macropore diameter
549 (excluding pores with a diameter $< 30 \mu\text{m}$) of each block using scanning electron microscope
550 images and open-source image analysis software ImageJ (data available in Table 4). The
551 average equivalent macropore diameter, $2r$, was calculated using $2r = 3/2(d_F)$, where d_F is
552 the average macropore Feret diameter. An example of how the average equivalent macropore
553 diameter was determined is available as Supplementary Information. Values of dry and wet K_{IC}
554 were then estimated using Equation (1), taking the average values of dry and wet UCS for each

555 block (Table 2). Dry and wet K_{IC} , and the wet to dry K_{IC} ratio, are plotted as a function of
556 alteration in Figures 9a and 9b, respectively (data available in Table 4). The data of Figure 9
557 highlight that (1) wet K_{IC} is lower than dry K_{IC} and (2) the reduction in K_{IC} in the presence of
558 water is increased as a function of increasing alteration. Using this approach, the wet to dry K_{IC}
559 ratio for the andesites studied herein is estimated to be between 0.32 and 0.93 (Figure 9). For
560 the most part, these values are lower than those typically reported in published studies. For
561 example, ratios for a suite of sandstones were measured to be between 0.65 and 0.95 (Noël et
562 al., 2021), and the ratio for an unaltered andesite (Kumamoto andesite) was measured to be 0.87
563 (Nara et al., 2012). We emphasise that the values of K_{IC} provided in Figure 9 and Table 4 are
564 estimates made using the pore-emanating crack model (Equation (1)), and not measured values
565 of K_{IC} as in Noël et al. (2021) and Nara et al. (2012).

566 A reduction in the K_{IC} of rocks in the presence of water has been observed by many
567 experimental studies and has been attributed to several, potentially coeval, factors: a reduction
568 in surface energy due to water adsorption (Baud et al., 2000; Noël et al., 2021), crack-tip
569 capillary forces (Nara et al., 2012), grain-contact lubrication (Guha Roy et al., 2017), stress
570 corrosion cracking (Kataoka et al., 2015), mineral dissolution (Maruvanchery and Kim, 2019),
571 and the presence of clay minerals (Wang et al., 2007; Nara et al., 2012). The reduction in K_{IC}
572 in the presence of water observed here (Figure 9a), is likely due to a combination of these
573 mechanisms; although, given that we provide here the short-term mechanical strength (UCS
574 experiments performed at a strain rate of 10^{-5} s^{-1}), we anticipate only minor contributions from
575 stress corrosion cracking and mineral dissolution. We consider that the increase in the reduction
576 in K_{IC} in the presence of water as alteration increases (Figure 9b) is most likely explained by
577 the increasing abundance of hydrophilic minerals, such as alunite and clay minerals, as a
578 function of increasing alteration (Table 1). Hydrophilic minerals expand upon saturation with
579 water, resulting in a reduction in their mechanical resistance (Nara et al., 2012). We further note

580 that, if hydrophilic minerals expand upon saturation and reduce ϕ and/or r , then the K_{IC}
 581 estimated for the altered rocks using Equation (1) would be even lower than our estimations
 582 presented in Table 4 and Figure 9.

583 We conclude, therefore, that the water-weakening in the dome rocks measured herein
 584 (i.e. the reduction in UCS; Figures 4, 5, 6, and 8) is likely due to a reduction in K_{IC} in the
 585 presence of water (Figure 9a). The increase in water-weakening as a function of alteration
 586 (Figure 5b) can be explained by the decrease in the wet to dry K_{IC} ratio as the degree of
 587 alteration (i.e. the abundance of hydrophilic minerals) increases (Figure 9b). The higher the
 588 wt% of secondary minerals such as alunite and clay minerals, the more K_{IC} is reduced when the
 589 rock is wet, and the greater the macroscopic water-weakening.

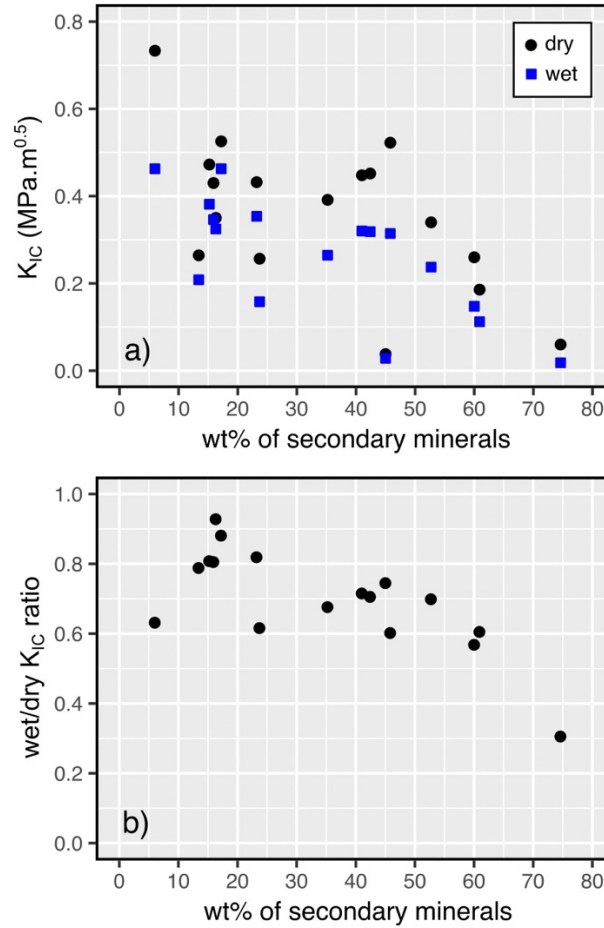
590

Sample	Weight percentage of secondary minerals	Average equivalent macropore diameter, r (μm)	Dry K_{IC} ($\text{MPa}\cdot\text{m}^{-1/2}$)	Wet K_{IC} ($\text{MPa}\cdot\text{m}^{-1/2}$)	Wet/dry K_{IC} ratio
H2A	23	179	0.43	0.35	0.82
H2B	75	173	0.06	0.02	0.31
H3	35	174	0.39	0.26	0.68
H4A	60	153	0.26	0.15	0.57
H5A	42	161	0.45	0.32	0.71
H6	53	145	0.34	0.24	0.70
H14	24	156	0.26	0.16	0.62
H15	61	180	0.19	0.11	0.60
H18	15	137	0.47	0.38	0.81
H20	45	167	0.04	0.03	0.74
H21	41	157	0.45	0.32	0.71
H22	17	88	0.53	0.46	0.88
H25	46	182	0.52	0.31	0.60
H29	16	204	0.43	0.35	0.81
H32	6	101	0.73	0.46	0.63
WP1285	13	69	0.26	0.21	0.79
WP1317	16	84	0.35	0.32	0.93

591

592 **Table 4.** Percentage of secondary minerals (i.e. alteration), average equivalent macropore
 593 diameter, wet fracture toughness (K_{IC}), dry K_{IC} , and the wet to dry K_{IC} ratio for the samples
 594 prepared for this study. Sample locations are provided in Figure 1b. Values of K_{IC} are
 595 estimated using the analytical approximation of Sammis and Ashby's (1986) pore-emanating

596 crack micromechanical model provided by Zhu et al. (2010) (Equation (1)). The relative
597 uncertainties in the quantification of the mineral contents (Table 1) are on the order of 5–10%.
598



599
600 **Figure 9.** (a) Fracture toughness (K_{IC}) and (b) the wet to dry K_{IC} ratio as a function of the
601 wt% of secondary minerals (i.e. alteration) for samples from La Soufrière de Guadeloupe
602 (Eastern Caribbean). Values of K_{IC} are estimated using the analytical approximation of
603 Sammis and Ashby's (1986) pore-emanating crack micromechanical model provided by Zhu
604 et al. (2010) (Equation (1)). The relative uncertainties in the quantification of the mineral
605 contents (Table 1) are on the order of 5–10%.

606
607 We highlight that we have performed experiments on completely dry and completely
608 water-saturated samples. However, in nature, the rocks forming a volcanic edifice or dome

609 likely exist between these two end-members (i.e. partially-saturated). Previous experimental
610 work has shown that the water-weakening observed at 100% saturation in sandstones can be
611 observed at saturation levels as low as 10%, whereas the compressive strength of shale
612 decreased almost linearly as a function of increasing saturation level (Schmitt et al., 1994).
613 Systematic uniaxial compressive strength measurements on partially-saturated volcanic rocks,
614 which preserve different porosities and alteration intensities, are now required to understand
615 whether the water-weakening observed here at 100% saturation (Figure 5) is also observed at
616 lower levels of saturation. Finally, we note that we have used deaired, deionised water for our
617 experiments. However, hydrothermal fluids, for example, are often characterised by low values
618 of pH (e.g., Delmelle et al., 2000) which can influence the short-term strength of rock (e.g.,
619 Singh et al., 1999). Future experimental studies should also explore the influence of fluid
620 composition and pH on the short-term strength of variably porous and variably altered volcanic
621 rock.

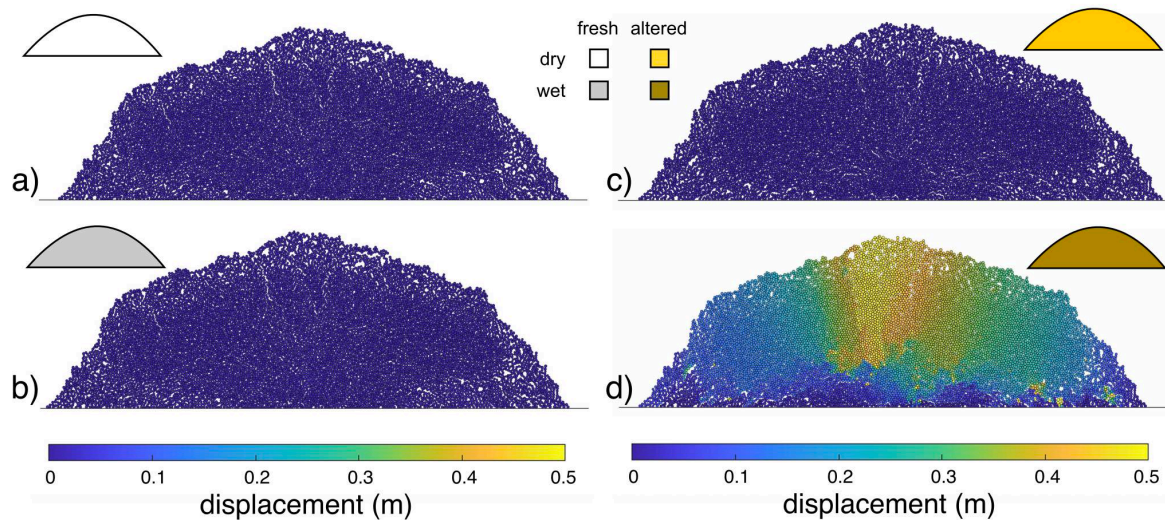
622

623 5.3 The influence of water-saturation on dome stability

624 We performed numerical simulations in PFC to better understand the influence of water-
625 saturation on dome stability. As explained in our methods section above, we first prepared
626 initially stable dry unaltered and altered domes, guided by our experimental data (Table 2). For
627 the dry unaltered dome, we determined the contact bond parameters required to give uniaxial
628 compressive strength, tensile strength, and Young's modulus values of 100 MPa, 10 MPa, and
629 25 GPa, respectively (Figure 10a). These values were chosen to represent the samples in our
630 dataset that are characterised by low levels of alteration (e.g., samples H18, H22, WP1317).
631 For the dry altered dome, we determined the contact bond parameters required to give uniaxial
632 compressive strength, tensile strength, and Young's modulus values of 10 MPa, 1 MPa, and 2
633 GPa, respectively (Figure 10c). These values were chosen to represent the samples in our

634 dataset that are characterised by high levels of alteration (e.g., sample H2B). We used a bulk
635 density of 2400 and 1500 kg/m³ for unaltered and altered dry rocks, respectively, as guided by
636 our experimental data. To investigate the influence of water-saturation at the dome scale, we
637 then changed all of the contact bond parameters in the model to those representative of wet
638 rocks (i.e. a completely water-saturated dome). Guided by our experimental data (Figures 5b
639 and 5d), we assumed wet to dry uniaxial compressive strength and Young's modulus ratios for
640 unaltered and altered dome rocks of 0.9 and 0.4, respectively. Therefore, we determined the
641 contact bond parameters required to give uniaxial compressive strength, tensile strength, and
642 Young's modulus of 90 MPa, 9 MPa, and 20 GPa, respectively, for the unaltered dome (Figure
643 10b) and, for the altered dome, we used values of 4 MPa, 0.4 MPa, and 1 GPa, respectively
644 (Figure 10d). We also note that, similar to the experimental data shown in Figure 3, the strain
645 required for failure in the model is also reduced upon saturation with water. Guided by our
646 experimental data, we used a bulk density of 2550 and 1900 kg/m³ for unaltered and altered
647 wet rocks, respectively. Finally, we highlight that, although alteration is thought to have
648 reduced the strength of the dome rocks from La Soufrière de Guadeloupe (Figure 4b; see also
649 discussions in Heap et al., 2021a, 2022a), alteration has also been observed, or inferred, to
650 increase the strength of volcanic rocks (e.g., Frolova et al., 2014; Pola et al., 2014; Wyering et
651 al., 2014; Coats et al., 2018; Heap et al., 2020b, 2021b; Kanakiya et al., 2021, 2022). Although
652 the rocks in these studies contain minerals such as kaolinite and alunite, minerals that may
653 promote water-weakening, it is unclear at present whether volcanic rocks that exhibit a
654 strengthening resulting from alteration would be, as seen for the rocks from La Soufrière de
655 Guadeloupe (Figures 4, 5, 6, and 8), weaker in the presence of water. As a result, until new
656 experimental data are available, the numerical modelling presented herein should be considered
657 applicable for scenarios in which alteration reduces strength.

658



659

660 **Figure 9.** A stable (i.e. no displacement) dome generated in Particle Flow Code (PFC) for a
 661 (a) dry unaltered dome and (c) dry altered dome. (b) The displacement in the dome shown in
 662 (a) resulting from changing the mechanical properties of the contacts in the stable dome to
 663 represent wet unaltered rock. (d) The displacement in the dome shown in (c) resulting from
 664 changing the mechanical properties of the contacts to represent wet altered rock. Blue - low
 665 displacement; yellow - high displacement.

666

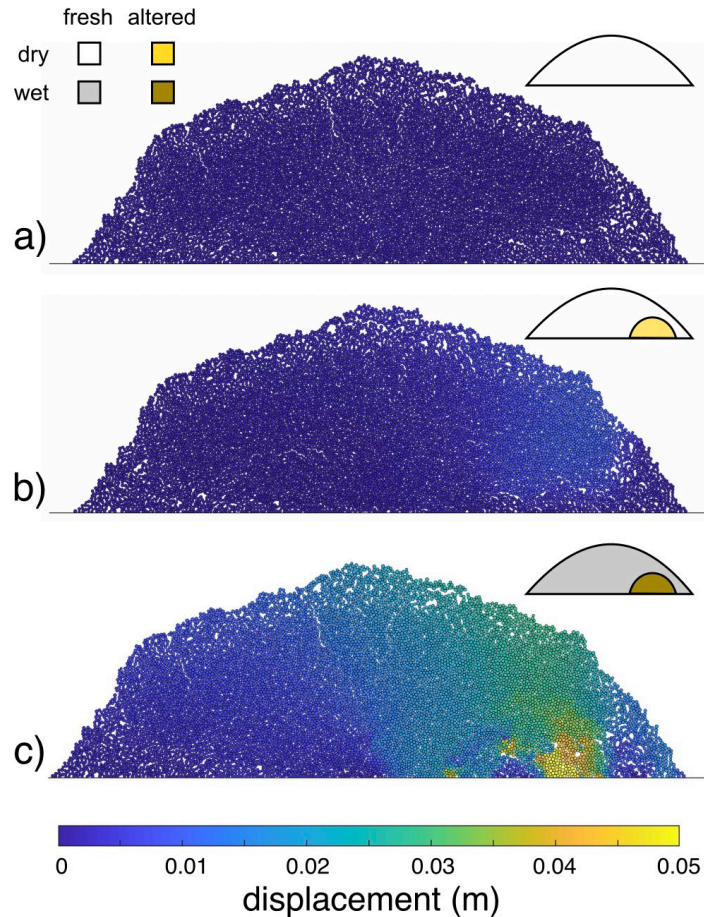
667 The results of the modelling show that displacements across the unaltered dome are
 668 essentially zero when the dome is water-saturated (Figure 10b), suggesting that water-saturation
 669 alone does not significantly influence the stability of an unaltered dome. By contrast,
 670 displacements are high (up to 0.5 m) when the altered dome is water-saturated, with the highest
 671 displacements concentrated at the centre of the dome (Figure 10d). Therefore, if an altered
 672 dome becomes saturated by, for example, heavy rainfall or rising hydrothermal fluids, the
 673 stability of the dome could be compromised, potentially promoting mass-wasting events (e.g.,
 674 partial dome collapse). We highlight that the propensity for such an altered water saturated
 675 dome to collapse will likely be significantly enhanced if the dome is resting on a sloping

676 substratum (see, for example, Harnett and Heap, 2021) or comprises listric low-strength layers
677 from previous partial flank collapses that are opened in the direction of maximum slope.

678 The scenarios shown in Figure 10 represent end-member scenarios in which the dome
679 is either completely unaltered or completely altered. In nature, hydrothermal alteration is likely
680 to be heterogeneously distributed within a dome (e.g., along permeable discontinuities).
681 Therefore, we performed additional modelling in which we included a buried altered zone
682 within an otherwise unaltered dome (Figure 11). In the first scenario, both the unaltered and
683 altered regions were dry (Figure 11b). In this scenario, only minor displacement is observed
684 within and above the buried altered zone (Figure 11b). In the second scenario, both the unaltered
685 and altered regions were water-saturated (Figure 11c). In this scenario, larger displacements are
686 observed within the altered zone, and notable displacements are also observed on the half of
687 the dome containing the buried alteration zone (Figure 11c). In other words, dome instability
688 was exacerbated following saturation in the presence of hydrothermally altered materials.
689 Therefore, the stability of a dome can be compromised by water-saturation (e.g., heavy rainfall,
690 changes to the hydrothermal system, and/or influx of seawater) even when only a small portion
691 of the dome is hydrothermally altered. It is likely, in this scenario, that dome stability would be
692 compromised more by alteration zones at or near the base of the dome, rather than at the top of
693 the dome.

694 The results of our modelling (Figures 10 and 11) may help explain why the frequency
695 of landslides and the failure and collapse of volcanic slopes and domes increases following
696 heavy rainfall (Kerle and van Wyk de Vries, 2001; Matthews et al., 2002; Matthews and
697 Barclay, 2004; Elsworth et al., 2004; Simmons et al., 2004; Taron et al., 2007; Saucedo et al.,
698 2008; Hicks et al., 2010; Vázquez et al., 2022).

699



700

701 **Figure 11.** (a) Stable (i.e. no displacement) dry altered dome generated in Particle Flow Code
702 (PFC). (b) The displacement in the dome shown in (a) resulting from adding a buried dry
703 alteration zone within a dry unaltered dome (as in Harnett et al., 2022). (c) The displacement
704 in the dome shown in (a) resulting from adding a buried wet alteration zone within a wet
705 unaltered dome. Blue - low displacement; yellow - high displacement.

706

707 Extreme or heavy rainfall has been linked to multiple volcanic hazards (McKee et al.,
708 1981; Matthews et al., 2002; Barclay et al., 2006), with theorised mechanisms that range from
709 deep-seated saturation and stress perturbations (McBirney, 1955; Violette et al., 2001;
710 Farquharson and Amelung, 2020; Sahoo et al., 2022) to shallow-seated processes operating in
711 the dome or upper edifice. Of these, the latter is often explained in terms of volumetric
712 expansion of liquids as a function of fuel-coolant interactions (Elsworth et al., 2004; Simmons

713 et al., 2004; Taron et al., 2007), with dome pressurisation and/or weakening driven by thermal
714 stress mechanisms (i.e. contraction of the dome carapace; Mastin, 1994; Yamasato et al., 1998;
715 Elsworth et al., 2004), or the stress on surrounding host-rock caused by the rapid growth of a
716 dome or cryptodome at shallow depth (Voight et al., 1981, 2002; Young et al., 2002). More
717 broadly, the saturation state of the edifice is thought to play an important role in volcano
718 destabilisation (McGuire, 1996; Day, 1996; Delcamp et al., 2016; Ball et al., 2018; Finn et al.,
719 2018; Heap et al., 2021b) and other failure processes, such as the failure of magma reservoirs
720 (Albino et al., 2018). Large-scale sector collapse events are also thought to be facilitated by
721 precipitation-induced retrogressive headward erosion and the weakening of former partial flank
722 collapse slip surfaces following precipitation (Kerle and van Wyk de Vries, 2001; Kerle et al.,
723 2003; Capra, 2006; Tost and Cronin, 2016; Romero et al., 2021). Our new data presented here
724 points to an additional role of dome or edifice rock saturation in promoting volcano instability,
725 in that saturation with water results in a reduction of rock strength of ~10–60% (Figure 5a).

726 The distribution and degree of hydrothermal alteration throughout a volcanic edifice is
727 also thought to be key in determining the potential for collapse-related hazards. Commonly
728 occurring hydrothermal mineral assemblages are thought to have a deleterious effect on volcano
729 stability (López and Williams, 1993; Watters et al., 2000; van Wyk de Vries et al., 2000; Reid
730 et al., 2001; Voight et al., 2002; Reid, 2004; Cecchi et al., 2004; Salaün et al., 2011; Ball et al.,
731 2015; Detienne et al., 2017; Norini et al., 2020; Heap et al., 2021a), as supported by
732 geomechanical studies on the role of hydrothermal alteration in reducing the strength of
733 volcanic materials (in both natural and laboratory settings; Moon and Jayawardane, 2004; de
734 Potro and Hürlimann, 2009; Pola et al., 2014; Wyering et al., 2014; Farquharson et al., 2019;
735 Mordensky et al., 2019; Heap et al., 2021a, 2022a; Darmawan et al., 2022). Indeed, structural
736 failure is often spatially coincident with hydrothermal alteration (Siebert et al., 1987; Delmelle
737 et al., 2015); for example, Zimbelman (1996) notes the association of alteration minerals—

738 including alunite, jarosite, and other sulphates—with exposed collapse scars, and Zimbelman
739 et al. (2005) link collapse events at andesitic arc volcanoes to veins of alteration minerals
740 resulting from the mixing of magmagenic sulphate and meteoric water. Indeed, Voight et al.
741 (2002) found varicoloured hydrothermally altered materials within avalanche deposits at
742 Soufrière Hills volcano (Montserrat, Eastern Caribbean). This link is congruent with
743 observations at La Soufrière de Guadeloupe, where avalanche deposits and material ejected
744 during phreatic explosions were found to contain various parts of the active and ancient
745 hydrothermal systems of the volcano (as evidenced by an acid-sulphate mineral assemblage;
746 Salaün et al., 2011; Heap et al., 2021a), and collapse events have revealed visibly altered
747 material beneath (see Figure 1b). La Soufrière de Guadeloupe is characterised by a vigorous
748 hydrothermal system (Komorowski et al., 2005; Villemant et al., 2005; Nicollin et al., 2006;
749 Coutant et al., 2012; Lesparre et al., 2012; Brothelande et al., 2014; Villemant et al., 2014;
750 Rosas-Carbajal et al., 2016, 2017; Moretti et al., 2020; Gibert et al., 2022) and, notably,
751 weathering fluxes on the volcano are among the highest recorded in tropical volcanic settings
752 (Dessert et al., 2015). Our new data underscore the importance of this hydrothermal alteration
753 on the mechanical properties of dome-forming rocks (Figure 5b), with UCS decreasing by as
754 much as ~60% upon water-saturation for highly altered materials (i.e. with a high proportion of
755 secondary minerals). These data further highlight how and why hydrothermal alteration and
756 water (meteoric, hydrothermal, or seawater) conspire to destabilise volcanic structures, as
757 outlined in disastrous effect by the 1998 collapse at Casita volcano (van Wyk de Vries et al.,
758 2000; Kerle and van Wyk de Vries, 2001; Kerle et al., 2003; Opfergelt et al., 2006) and several
759 large rain-triggered collapses during the period of active dome growth at Soufrière Hills
760 volcano (Elsworth et al., 2004; Simmons et al., 2004; Taron et al., 2007).

761 Based on observations of rainfall-induced dome instability at Soufrière Hills volcano,
762 previous research has focussed on developing mechanistic models of dome collapse as a

763 function of local rainfall rate (Elsworth et al., 2004; Matthews and Barclay, 2004; Taron et al.,
764 2007; see also Harnett et al., 2019) thereby—directly or indirectly—accounting for the
765 saturation state. In contrast, numerous studies that model the influence of alteration on dome or
766 flank stability do not consider the presence or absence of interstitial fluids on the mechanical
767 properties of the dome-forming materials. Critically, our modelling results (Figures 10 and 11)
768 demonstrate that mechanical failure is promoted when both hydrothermal alteration and water-
769 saturation operate in tandem. We emphasise that mechanical water-weakening is an important
770 additional mechanism that has generally not been considered in existing stability modelling of
771 domes, but that can facilitate collapse, particularly in the likely scenario when alteration is also
772 present (Figures 10 and 11). We suggest that, when appropriate and where available, volcano
773 stability models use data relevant for water-saturated volcanic rocks. We consider this
774 especially relevant for submarine, coastal, and ocean-island volcanoes. For the modelling of
775 coastal and ocean-island volcanoes, it is likely important to not only consider the partially
776 saturated subaerial part of the volcano, but also the saturated submarine part (the importance of
777 not neglecting the submarine portion of a coastal volcano is discussed in Urlaub et al., 2018).

778 We also highlight that the link between mechanical water-weakening and hydrothermal
779 alteration may also be further exacerbated when hot gases and rising hydrothermal/magmatic
780 fluids interact with water-saturated altered zones at shallow levels within a dome or volcano,
781 generating large volumes of steam and elevated fluid pore pressures. Indeed, previous
782 modelling has shown that elevated pore pressure negatively impacts volcano stability (Reid,
783 2004; Heap et al., 2021b). The rise of large volumes of hydrothermal fluids due to major heat
784 pulses was observed during all phreatic unrest and eruptions at La Soufrière of Guadeloupe
785 (Komorowski et al., 2005; Rosas-Carbajal et al., 2016) and Mount Pelée in 1902 (Tanguy,
786 1994), and is characteristic of the ongoing unrest at La Soufrière of Guadeloupe (Moretti et al.,

787 2020), underscoring the importance of incorporating these phenomena into future, more
788 complex volcano stability models.

789 By combining our experimental results with analytical and numerical mechanical
790 modelling, we link the micro-scale effects of hydrothermal alteration on the fracture mechanics
791 to the scale of the dome. These considerations are particularly important in light of projected
792 climate futures (Aubry et al., 2022). As circulation models results in Figure 1c highlight, La
793 Soufrière de Guadeloupe is projected to receive increasing amounts of heavy rainfall over the
794 next 80 years (see also Cantet et al., 2014), even given widespread adoption of stringent climate
795 change mitigation policies. Accordingly, the propensity for rainfall-induced collapse events
796 will likely increase as well, and detecting where potential collapse events may occur becomes
797 ever more crucial, especially given the absence of detectable geophysical signals preceding
798 such events (Matthews et al., 2002). Our model results highlight that identifying zones of
799 (potentially concealed) hydrothermal alteration may prove to be key in mitigating such hazards
800 (Darmawan et al., 2022; Harnett et al., 2022). Moreover, our results emphasise that close
801 monitoring of domes and slopes during and following heavy rainfall is essential: we echo the
802 call of Barclay et al. (2006) for routine incorporation of meteorological data into monitoring
803 praxis. Finally, direct knowledge of the state of edifice or dome saturation could be invaluable
804 for future stability monitoring. Our new data and models add a new importance to the 3D
805 characterisation of water saturation in volcanic edifices, as well as its evolution over time, using
806 geophysical methods. For example, geophysical methods such as electrical resistivity
807 tomography (e.g. Rosas-Carbajal et al., 2016) and muon tomography (Rosas-Carbajal et al.,
808 2017; Bajou et al., 2023) are sensitive to water content and could be repeatedly employed to
809 assess the distribution of water in the upper parts of the volcanic edifice. Both seismic noise
810 interferometry (Sens-Schönfelder and Wegler, 2006), a method increasingly used to monitor
811 water level variations, and the satellite-based monitoring of groundwater (Rodell et al., 2009)

812 could also be powerful tools to track edifice or dome saturation. Finally, borehole dilatometers
813 and piezometers (Hurwitz and Johnston, 2003) could provide punctual and precise data to
814 calibrate numerical models and interpret geophysical imaging.

815 While La Soufrière de Guadeloupe has been chosen as a case study herein, for the
816 reasons outlined in section two, we emphasise that our conclusions are much more broadly
817 applicable. Volcanoes exhibiting zones of intense alteration and/or vigorous hydrothermal
818 systems (Africano and Bernard, 2000; Zimelman et al., 2005; Rodríguez and van Bergen,
819 2017; Yilmaz et al., 2021), as well as those with persistent acid lakes (van Hinsberg et al., 2010;
820 Rouwet et al., 2014; Delmelle et al., 2015), will likely be particularly prone to extensive water-
821 weakening, and therefore heightened instability, in the event of edifice and/or dome saturation.
822 In tropical environments, increasingly frequent bouts of intense precipitation (not only during
823 the so-called hurricane or rainy season but also at other times of the year in the Tropics) may
824 directly trigger mass-wasting events (as observed elsewhere in the Caribbean: Matthews et al.,
825 2002; Carn et al., 2004; Taron et al., 2007; Matthews et al., 2009 and in other settings: Yamasato
826 et al., 1998; Elsworth et al., 2004), or facilitate other internal or external trigger mechanisms
827 such as magma movement (Reid et al., 2010), pressurisation (Reid, 2004; Heap et al., 2021b),
828 or basal spreading (van Wyk de Vries and Francis, 1997). For the majority of subaerial
829 volcanoes, climate models project an increase in such meteorological events (Farquharson and
830 Amelung, 2022). In the context of water-weakening and related hazards, climate change may
831 also be important in terms of sea level rise. Analysis of drill cores from offshore Montserrat
832 shows that Soufrière Hills volcano underwent periods of heightened instability during periods
833 of rapid sea level rise, with all three large collapse events at the volcano being correlated with
834 sea level changes of > 5 m/ka (Coussens et al., 2016); those authors also highlight that this
835 phenomenon appears to echo a broader trend across other island arc volcanoes. We further posit

836 that variation in edifice saturation due to sea level rise could also promote instability in coastal
837 or island arc volcanoes.

838

839 **6 Conclusions**

840 The goal of this study, using dome stability models informed by experimental data, was
841 to investigate whether water-saturation alone can jeopardise the stability of a lava dome. Our
842 experiments show that water-saturation reduced the strength of variably-altered dome rocks,
843 and that water-weakening increased as the degree of alteration increased. Micromechanical
844 modelling suggested that the observed water-weakening was the result of a decrease in fracture
845 toughness, K_{IC} , in the presence of water. The ratio of wet to dry K_{IC} also decreased with
846 increasing alteration, explaining the trend of increasing water-weakening with increasing
847 alteration. Dome stability modelling, informed by our experimental data, showed that the
848 stability of a lava dome can be compromised by water-saturation if the dome is altered, or
849 contains an altered zone (even without the compounding exacerbating effects of volcanic
850 unrest, such as seismicity, deformation, high heat fluxes, and rising fluids). The models
851 presented herein may therefore help explain why the frequency of landslides and the failure and
852 collapse of altered volcanic slopes and dome increases following heavy rainfall. Our study
853 highlights, and especially in the light of predicted increases in heavy rainfall due to climate
854 change, that the degree of alteration and water-saturation should be monitored at active
855 volcanoes worldwide, volcanic domes and slopes should be closely monitored following heavy
856 rainfall, and that large-scale volcano stability models should use values for water-saturated
857 rocks where and when appropriate.

858

859 **Acknowledgements**

860 This work was supported by ANR grant MYGALE (“Modelling the phYsical and
861 chemical Gradients of hydrothermal ALteration for warning systems of flank collapse at
862 Explosive volcanoes”; ANR-21-CE49-0010). M. Heap also acknowledges support from the
863 Institut Universitaire de France (IUF). We thank Tomaso Esposti Ongaro and Lucille Carbillet
864 for help in the field, Laurent Gastaldo and Bertrand Renaudie for help in the laboratory, and all
865 those working at the Observatoire Volcanologique et Sismologique de Guadeloupe (OVSG).
866 This research was also supported by two Hubert Curien Partnership (PHC) grants: a Germaine
867 de Staël grant awarded to M. Heap and M. Violay (grant number 47712SB) and a Ulysses grant
868 awarded to M. Heap and C. Harnett (grant number 47199ZM). The Germaine de Staël grant is
869 implemented by the Ministry for Higher Education, Research, and Innovation (MESRI) and the
870 Ministry for Europe and Foreign Affairs (MEAE) in France, and by the State Secretariat for
871 Education, Research, and Innovation (SERI) and the Swiss Academy of Technical Sciences
872 (SATW) in Switzerland. The Ulysses grant is implemented by the MEAE and the MESRI in
873 France, and by the Irish Research Council (IRC) in Ireland. This research also benefitted from
874 European Research Council Starting Grant BEFINE (ERC-2017-STG), awarded to M. Violay.
875 We thank the IPGP for general funding for the Observatoires Volcanologiques et
876 Sismologiques (OVS), INSU-CNRS for the funding provided to the Service National
877 d’Observation en Volcanologie (SNOV), and the Ministère pour la Transition Ecologique
878 (MTE) for financial support for the monitoring of the unstable flank of La Soufrière de
879 Guadeloupe. We are grateful to the Parc National de la Guadeloupe for allowing us to carry out
880 geological fieldwork on La Soufrière de Guadeloupe. Finally, we thank The Fleet (Dublin,
881 Ireland) for their hospitality. The constructive comments of Shane Cronin, Ludmila Adam, and
882 Anthony Lamur helped improve this manuscript.

883

884 **References**

885 Africano, F., & Bernard, A. (2000). Acid alteration in the fumarolic environment of Usu volcano, Hokkaido, Japan.
886 *Journal of Volcanology and Geothermal Research*, 97(1-4), 475-495.

887 Aizawa, K., Ogawa, Y., & Ishido, T. (2009). Groundwater flow and hydrothermal systems within volcanic
888 edifices: Delineation by electric self-potential and magnetotellurics. *Journal of Geophysical Research:*
889 *Solid Earth*, 114(B1).

890 Albino, F., Amelung, F., & Gregg, P. (2018). The role of pore fluid pressure on the failure of magma reservoirs:
891 insights from Indonesian and Aleutian arc volcanoes. *Journal of Geophysical Research: Solid Earth*, 123(2),
892 1328-1349.

893 Allemand, P., Delacourt, C., Lajeunesse, E., Devauchelle, O., & Beauducel, F. (2014). Erosive effects of the storm
894 Helena (1963) on Basse Terre Island (Guadeloupe—Lesser Antilles Arc). *Geomorphology*, 206, 79-86.

895 Apuani, T., Corazzato, C., Cancelli, A., & Tibaldi, A. (2005). Stability of a collapsing volcano (Stromboli, Italy):
896 Limit equilibrium analysis and numerical modelling. *Journal of Volcanology and Geothermal Research*,
897 144(1-4), 191-210.

898 Atkinson, B. K. (1984). Subcritical crack growth in geological materials. *Journal of Geophysical Research: Solid*
899 *Earth*, 89(B6), 4077-4114.

900 Aubry, T. J., Farquharson, J. I., Rowell, C. R., Watt, S. F., Pinel, V., Beckett, F., ... & Sykes, J. S. (2022). Impact
901 of climate change on volcanic processes: current understanding and future challenges. *Bulletin of*
902 *Volcanology*, 84(6), 58.

903 Bajou, R., Rosas-Carbajal, M., Tonazzo, A., & Marteau, J. (2023). High-resolution structural imaging of volcanoes
904 using improved muon tracking. *Geophysical Journal International*, 235(2), 1138-1149.

905 Ball, J. L., Stauffer, P. H., Calder, E. S., & Valentine, G. A. (2015). The hydrothermal alteration of cooling lava
906 domes. *Bulletin of Volcanology*, 77, 1-16.

907 Ball, J. L., Taron, J., Reid, M. E., Hurwitz, S., Finn, C., & Bedrosian, P. (2018). Combining multiphase
908 groundwater flow and slope stability models to assess stratovolcano flank collapse in the Cascade Range.
909 *Journal of Geophysical Research: Solid Earth*, 123(4), 2787-2805.

910 Barclay, J., Johnstone, J. E., & Matthews, A. J. (2006). Meteorological monitoring of an active volcano:
911 implications for eruption prediction. *Journal of volcanology and geothermal research*, 150(4), 339-358.

912 Baud, P., Zhu, W., & Wong, T. F. (2000). Failure mode and weakening effect of water on sandstone. *Journal of*
913 *Geophysical Research: Solid Earth*, 105(B7), 16371-16389.

914 Baud, P., Reuschlé, T., Ji, Y., Cheung, C. S., & Wong, T. F. (2015). Mechanical compaction and strain localization
915 in Bleurswiller sandstone. *Journal of Geophysical Research: Solid Earth*, 120(9), 6501-6522.

916 Baud, P., Rolland, A., Heap, M., Xu, T., Nicolé, M., Ferrand, T., ... & Conil, N. (2016). Impact of stylolites on the
917 mechanical strength of limestone. *Tectonophysics*, 690, 4-20.

918 Borselli, L., Capra, L., Sarocchi, D., & De la Cruz-Reyna, S. (2011). Flank collapse scenarios at Volcán de Colima,
919 Mexico: a relative instability analysis. *Journal of Volcanology and Geothermal Research*, 208(1-2), 51-65.

920 Boudon, G., Komorowski, J. C., Villemant, B., & Semet, M. P. (2008). A new scenario for the last magmatic
921 eruption of La Soufrière de Guadeloupe (Lesser Antilles) in 1530 AD Evidence from stratigraphy
922 radiocarbon dating and magmatic evolution of erupted products. *Journal of Volcanology and Geothermal*
923 *Research*, 178(3), 474-490.

924 Brantut, N., Heap, M. J., Meredith, P. G., & Baud, P. (2013). Time-dependent cracking and brittle creep in crustal
925 rocks: A review. *Journal of Structural Geology*, 52, 17-43.

926 Brombach, T., Marini, L., & Hunziker, J. C. (2000). Geochemistry of the thermal springs and fumaroles of Basse-
927 Terre Island, Guadeloupe, Lesser Antilles. *Bulletin of Volcanology*, 61, 477-490.

928 Brothelande, E., Finizola, A., Peltier, A., Delcher, E., Komorowski, J. C., Di Gangi, F., ... & Legendre, Y. (2014).
929 Fluid circulation pattern inside La Soufrière volcano (Guadeloupe) inferred from combined electrical
930 resistivity tomography, self-potential, soil temperature and diffuse degassing measurements. *Journal of*
931 *Volcanology and Geothermal Research*, 288, 105-122.

932 de Bremond d'Ars, J., & Gibert, D. (2022). Multiscale external rainfall forcing from high-resolution temperature
933 time series of fumaroles at La Soufrière de Guadeloupe volcano. *Frontiers in Earth Science*, 9, 1364.

934 del Potro, R., & Hürliemann, M. (2009). The decrease in the shear strength of volcanic materials with argillic
935 hydrothermal alteration, insights from the summit region of Teide stratovolcano, Tenerife. *Engineering*
936 *Geology*, 104(1-2), 135-143.

937 Cantet, P., Déqué, M., Palany, P., & Maridet, J. L. (2014). The importance of using a high-resolution model to
938 study the climate change on small islands: the Lesser Antilles case. *Tellus A: Dynamic Meteorology and*
939 *Oceanography*, 66(1), 24065.

940 Capra, L. (2006). Abrupt climatic changes as triggering mechanisms of massive volcanic collapses. *Journal of*
941 *Volcanology and Geothermal Research*, 155(3-4), 329-333.

942 Carn, S. A., Watts, R. B., Thompson, G., & Norton, G. E. (2004). Anatomy of a lava dome collapse: the 20 March
943 2000 event at Soufrière Hills Volcano, Montserrat. *Journal of Volcanology and Geothermal Research*,
944 131(3-4), 241-264.

- 945 Carr, B. B., Lev, E., Vanderkluyzen, L., Moyer, D., Marliyani, G. I., & Clarke, A. B. (2022). The stability and
946 collapse of lava domes: Insight from photogrammetry and slope stability models applied to Sinabung
947 volcano (Indonesia). *Frontiers in Earth Science*, 10, 813813.
- 948 Caselle, C., Baud, P., Kushnir, A. R. L., Reuschlé, T., & Bonetto, S. M. R. (2022). Influence of water on
949 deformation and failure of gypsum rock. *Journal of Structural Geology*, 163, 104722.
- 950 Castagna, A., Ougier-Simonin, A., Benson, P. M., Browning, J., Walker, R. J., Fazio, M., & Vinciguerra, S. (2018).
951 Thermal damage and pore pressure effects of the Brittle-Ductile transition in comiso limestone. *Journal of*
952 *Geophysical Research: Solid Earth*, 123(9), 7644-7660.
- 953 Cecchi, E., van Wyk de Vries, B., & Lavest, J. M. (2004). Flank spreading and collapse of weak-cored volcanoes.
954 *Bulletin of Volcanology*, 67, 72-91.
- 955 Chester, F. M., & Logan, J. M. (1986). Implications for mechanical properties of brittle faults from observations
956 of the Punchbowl fault zone, California. *Pure and Applied Geophysics*, 124, 79-106.
- 957 Coats, R., Kendrick, J. E., Wallace, P. A., Miwa, T., Hornby, A. J., Ashworth, J. D., ... & Lavallée, Y. (2018).
958 Failure criteria for porous dome rocks and lavas: a study of Mt. Unzen, Japan. *Solid Earth*, 9, 1299-1328.
- 959 Coussens, M., Wall-Palmer, D., Talling, P. J., Watt, S. F., Cassidy, M., Jutzeler, M., ... & Stinton, A. J. (2016).
960 The relationship between eruptive activity, flank collapse, and sea level at volcanic islands: A long-term (>
961 1 Ma) record offshore Montserrat, Lesser Antilles. *Geochemistry, Geophysics, Geosystems*, 17(7), 2591-
962 2611.
- 963 Coutant, O., Bernard, M. L., Beauducel, F., Nicollin, F., Bouin, M. P., & Roussel, S. (2012). Joint inversion of P-
964 wave velocity and density, application to La Soufrière of Guadeloupe hydrothermal system. *Geophysical*
965 *Journal International*, 191(2), 723-742.
- 966 Darmawan, H., Troll, V. R., Walter, T. R., Deegan, F. M., Geiger, H., Heap, M. J., ... & Müller, D. (2022). Hidden
967 mechanical weaknesses within lava domes provided by buried high-porosity hydrothermal alteration zones.
968 *Scientific Reports*, 12(1), 3202.
- 969 Day, S. J. (1996). Hydrothermal pore fluid pressure and the stability of porous, permeable volcanoes. *Geological*
970 *Society, London, Special Publications*, 110(1), 77-93.
- 971 Delcamp, A., Roberti, G., & van Wyk de Vries, B. (2016). Water in volcanoes: evolution, storage and rapid release
972 during landslides. *Bulletin of Volcanology*, 78, 1-12.
- 973 Delmelle, P., Bernard, A., Kusakabe, M., Fischer, T. P., & Takano, B. (2000). Geochemistry of the magmatic-
974 hydrothermal system of Kawah Ijen volcano, East Java, Indonesia. *Journal of Volcanology and Geothermal*
975 *research*, 97(1-4), 31-53.
- 976 Delmelle, P., Henley, R. W., Opfergelt, S., & Detienne, M. (2015). Summit acid crater lakes and flank instability
977 in composite volcanoes. *Volcanic lakes*, 289-305.
- 978 Dessert, C., Lajeunesse, E., Lloret, E., Clergue, C., Crispi, O., Gorge, C., & Quidelleur, X. (2015). Controls on
979 chemical weathering on a mountainous volcanic tropical island: Guadeloupe (French West Indies).
980 *Geochimica et Cosmochimica Acta*, 171, 216-237.
- 981 Detienne, M., Delmelle, P., Guevara, A., Samaniego, P., Opfergelt, S., & Mothes, P. A. (2017). Contrasting origin
982 of two clay-rich debris flows at Cayambe Volcanic Complex, Ecuador. *Bulletin of Volcanology*, 79, 1-14.
- 983 Duda, M., & Renner, J. (2013). The weakening effect of water on the brittle failure strength of sandstone.
984 *Geophysical Journal International*, 192(3), 1091-1108.
- 985 Elsworth, D., Voight, B., Thompson, G., & Young, S. R. (2004). Thermal-hydrologic mechanism for rainfall-
986 triggered collapse of lava domes. *Geology*, 32(11), 969-972.
- 987 Farquharson, J. I., Wild, B., Kushnir, A. R., Heap, M. J., Baud, P., & Kennedy, B. (2019). Acid-induced dissolution
988 of andesite: evolution of permeability and strength. *Journal of Geophysical Research: Solid Earth*, 124(1),
989 257-273.
- 990 Farquharson, J. I., & Amelung, F. (2020). Extreme rainfall triggered the 2018 rift eruption at Kīlauea Volcano.
991 *Nature*, 580(7804), 491-495.
- 992 Farquharson, J. I., & Amelung, F. (2022). Volcanic hazard exacerbated by future global warming-driven increase
993 in heavy rainfall. *Royal Society Open Science*, 9(7), 220275.
- 994 Finn, C. A., Deszcz-Pan, M., Ball, J. L., Bloss, B. J., & Minsley, B. J. (2018). Three-dimensional geophysical
995 mapping of shallow water saturated altered rocks at Mount Baker, Washington: Implications for slope
996 stability. *Journal of Volcanology and Geothermal Research*, 357, 261-275.
- 997 Frolova, J., Ladygin, V., Rychagov, S., & Zukhubaya, D. (2014). Effects of hydrothermal alterations on physical
998 and mechanical properties of rocks in the Kuril-Kamchatka island arc. *Engineering Geology*, 183, 80-95.
- 999 Frolova, J. V., Chernov, M. S., Rychagov, S. N., Ladygin, V. M., Sokolov, V. N., & Kuznetsov, R. A. (2021). The
1000 influence of hydrothermal argillization on the physical and mechanical properties of tuffaceous rocks: a
1001 case study from the Upper Pauzhetsky thermal field, Kamchatka. *Bulletin of Engineering Geology and the*
1002 *Environment*, 80, 1635-1651.
- 1003 Fulignati, P. (2020). Clay minerals in hydrothermal systems. *Minerals*, 10(10), 919.

- 1004 Gibert, D., de Bremond d'Ars, J., Carlus, B., Deroussi, S., Ianigro, J. C., Jessop, D. E., ... & Rosas-Carbajal, M.
1005 (2022). Observation of the Dynamics of Hydrothermal Activity in La Soufrière of Guadeloupe Volcano
1006 with Joint Muography, Gravimetry, Electrical Resistivity Tomography, Seismic and Temperature
1007 Monitoring. *Muography: Exploring Earth's Subsurface with Elementary Particles*, 55-73.
- 1008 Guha Roy, D., Singh, T. N., Kodikara, J., & Talukdar, M. (2017). Correlating the mechanical and physical
1009 properties with mode-I fracture toughness of rocks. *Rock Mechanics and Rock Engineering*, 50, 1941-1946.
- 1010 Harnett, C. E., Thomas, M. E., Purvance, M. D., & Neuberg, J. (2018). Using a discrete element approach to model
1011 lava dome emplacement and collapse. *Journal of Volcanology and Geothermal Research*, 359, 68-77.
- 1012 Harnett, C. E., Kendrick, J. E., Lamur, A., Thomas, M. E., Stinton, A., Wallace, P. A., ... & Lavallée, Y. (2019).
1013 Evolution of mechanical properties of lava dome rocks across the 1995–2010 eruption of soufrière hills
1014 volcano, Montserrat. *Frontiers in Earth Science*, 7, 7.
- 1015 Harnett, C. E., & Heap, M. J. (2021). Mechanical and topographic factors influencing lava dome growth and
1016 collapse. *Journal of Volcanology and Geothermal Research*, 420, 107398.
- 1017 Harnett, C. E., Heap, M. J., Troll, V. R., Deegan, F. M., & Walter, T. R. (2022). Large-scale lava dome fracturing
1018 as a result of concealed weakened zones. *Geology*, 50(12), 1346-1350.
- 1019 Hawkins, A. B., & McConnell, B. J. (1992). Sensitivity of sandstone strength and deformability to changes in
1020 moisture content. *Quarterly Journal of Engineering Geology*, 25(2), 115-130.
- 1021 Heap, M. J., Kennedy, B. M., Pernin, N., Jacquemard, L., Baud, P., Farquharson, J. I., ... & Dingwell, D. B. (2015).
1022 Mechanical behaviour and failure modes in the Whakaari (White Island volcano) hydrothermal system,
1023 New Zealand. *Journal of Volcanology and Geothermal Research*, 295, 26-42.
- 1024 Heap, M. J., Farquharson, J. I., Kushnir, A. R., Lavallée, Y., Baud, P., Gilg, H. A., & Reuschlé, T. (2018). The
1025 influence of water on the strength of Neapolitan Yellow Tuff, the most widely used building stone in Naples
1026 (Italy). *Bulletin of Volcanology*, 80, 1-15.
- 1027 Heap, M. J., Villeneuve, M., Kushnir, A. R., Farquharson, J. I., Baud, P., & Reuschlé, T. (2019). Rock mass
1028 strength and elastic modulus of the Buntsandstein: an important lithostratigraphic unit for geothermal
1029 exploitation in the Upper Rhine Graben. *Geothermics*, 77, 236-256.
- 1030 Heap, M. J., Villeneuve, M., Albino, F., Farquharson, J. I., Brothelande, E., Amelung, F., ... & Baud, P. (2020a).
1031 Towards more realistic values of elastic moduli for volcano modelling. *Journal of Volcanology and
1032 Geothermal Research*, 390, 106684.
- 1033 Heap, M. J., Gravley, D. M., Kennedy, B. M., Gilg, H. A., Bertolett, E., & Barker, S. L. (2020b). Quantifying the
1034 role of hydrothermal alteration in creating geothermal and epithermal mineral resources: The Ohakuri
1035 ignimbrite (Taupō Volcanic Zone, New Zealand). *Journal of Volcanology and Geothermal Research*, 390,
1036 106703.
- 1037 Heap, M. J., Baumann, T. S., Rosas-Carbajal, M., Komorowski, J. C., Gilg, H. A., Villeneuve, M., ... & Reuschlé,
1038 T. (2021a). Alteration-Induced Volcano Instability at La Soufrière de Guadeloupe (Eastern Caribbean).
1039 *Journal of Geophysical Research: Solid Earth*, 126(8), e2021JB022514.
- 1040 Heap, M. J., Baumann, T., Gilg, H. A., Kolzenburg, S., Ryan, A. G., Villeneuve, M., ... & Clynne, M. A. (2021b).
1041 Hydrothermal alteration can result in pore pressurization and volcano instability. *Geology*, 49(11), 1348-
1042 1352.
- 1043 Heap, M. J., & Violay, M. E. (2021). The mechanical behaviour and failure modes of volcanic rocks: a review.
1044 *Bulletin of Volcanology*, 83(5), 33.
- 1045 Heap, M. J., Harnett, C. E., Wadsworth, F. B., Gilg, H. A., Carbillet, L., Rosas-Carbajal, M., ... & Moretti, R.
1046 (2022a). The tensile strength of hydrothermally altered volcanic rocks. *Journal of Volcanology and
1047 Geothermal Research*, 428, 107576.
- 1048 Heap, M. J., Jessop, D. E., Wadsworth, F. B., Rosas-Carbajal, M., Komorowski, J. C., Gilg, H. A., ... & Moretti,
1049 R. (2022b). The thermal properties of hydrothermally altered andesites from La Soufrière de Guadeloupe
1050 (Eastern Caribbean). *Journal of Volcanology and Geothermal Research*, 421, 107444.
- 1051 Heap, M. J., Troll, V. R., Harris, C., Gilg, H. A., Moretti, R., Rosas-Carbajal, M., ... & Baud, P. (2022c). Whole-
1052 rock oxygen isotope ratios as a proxy for the strength and stiffness of hydrothermally altered volcanic rocks.
1053 *Bulletin of Volcanology*, 84(8), 74.
- 1054 Heap, M. J., Harnett, C. E., Nazarbayov, T., Heng, Z., Baud, P., Xu, T., ... & Komorowski, J. C. (2023a). The
1055 influence of heterogeneity on the strength of volcanic rocks and the stability of lava domes. *Bulletin of
1056 Volcanology*, 85(9), 49.
- 1057 Heap, M. J., Wadsworth, F. B., & Jessop, D. E. (2023b). The thermal conductivity of unlithified granular volcanic
1058 materials: The influence of hydrothermal alteration and degree of water saturation. *Journal of Volcanology
1059 and Geothermal Research*, 107775.
- 1060 Hicks, P. D., Matthews, A. J., & Cooker, M. J. (2010). Triggering of a volcanic dome collapse by rainwater
1061 infiltration. *Journal of Geophysical Research: Solid Earth*, 115(B9).

- 1062 Hurwitz, S., Kipp, K. L., Ingebritsen, S. E., & Reid, M. E. (2003). Groundwater flow, heat transport, and water
1063 table position within volcanic edifices: Implications for volcanic processes in the Cascade Range. *Journal*
1064 *of Geophysical Research: Solid Earth*, 108(B12).
- 1065 Husain, T., Elsworth, D., Voight, B., Mattioli, G., & Jansma, P. (2014). Influence of extrusion rate and magma
1066 rheology on the growth of lava domes: Insights from particle-dynamics modeling. *Journal of volcanology*
1067 *and geothermal research*, 285, 100-117.
- 1068 Husain, T., Elsworth, D., Voight, B., Mattioli, G., & Jansma, P. (2018). Influence of conduit flow mechanics on
1069 magma rheology and the growth style of lava domes. *Geophysical Journal International*, 213(3), 1768-
1070 1784.
- 1071 Husain, T., Elsworth, D., Voight, B., Mattioli, G., & Jansma, P. (2019). Morphologic variation of an evolving
1072 dome controlled by the extrusion of finite yield strength magma. *Journal of Volcanology and Geothermal*
1073 *Research*, 370, 51-64.
- 1074 Inoue, A. (1995). Formation of clay minerals in hydrothermal environments. *Origin and Mineralogy of Clays:*
1075 *Clays and the Environment*, 268-329.
- 1076 Jessop, D. E., Moune, S., Moretti, R., Gibert, D., Komorowski, J. C., Robert, V., ... & Burtin, A. (2021). A multi-
1077 decadal view of the heat and mass budget of a volcano in unrest: La Soufrière de Guadeloupe (French West
1078 Indies). *Bulletin of Volcanology*, 83, 1-19.
- 1079 Join, J. L., Folio, J. L., & Robineau, B. (2005). Aquifers and groundwater within active shield volcanoes. Evolution
1080 of conceptual models in the Piton de la Fournaise volcano. *Journal of Volcanology and Geothermal*
1081 *Research*, 147(1-2), 187-201.
- 1082 Kanakiya, S., Adam, L., Rowe, M. C., Lindsay, J. M., & Esteban, L. (2021). The role of tuffs in sealing volcanic
1083 conduits. *Geophysical Research Letters*, 48(20), e2021GL095175.
- 1084 Kanakiya, S., Adam, L., Rowe, M. C., Esteban, L., Lerner, G. A., & Lindsay, J. M. (2022). Petrophysical and
1085 elastic properties of altered lavas from Mt. Taranaki: Implications for dome stability. *Journal of*
1086 *Volcanology and Geothermal Research*, 432, 107693.
- 1087 Kataoka, M., Obara, Y., & Kuruppu, M. (2015). Estimation of fracture toughness of anisotropic rocks by semi-
1088 circular bend (SCB) tests under water vapor pressure. *Rock Mechanics and Rock Engineering*, 48, 1353-
1089 1367.
- 1090 Kendrick, J. E., Schaefer, L. N., Schauthroth, J., Bell, A. F., Lamb, O. D., Lamur, A., ... & Kennedy, B. M. (2021).
1091 Physical and mechanical rock properties of a heterogeneous volcano: the case of Mount Unzen, Japan.
1092 *Solid Earth*, 12(3), 633-664.
- 1093 Kerle, N., & De Vries, B. V. W. (2001). The 1998 debris avalanche at Casita volcano, Nicaragua—investigation
1094 of structural deformation as the cause of slope instability using remote sensing. *Journal of Volcanology and*
1095 *Geothermal Research*, 105(1-2), 49-63.
- 1096 Kerle, N., van Wyk de Vries, B., & Oppenheimer, C. (2003). New insight into the factors leading to the 1998 flank
1097 collapse and lahar disaster at Casita volcano, Nicaragua. *Bulletin of volcanology*, 65, 331-345.
- 1098 Komorowski, J.-C., Boudon, G., Semet, M., Beauducel, F., Anténor-Habazac, C., Bazin, S., & Hammouya, G.
1099 (2005). Guadeloupe. In J. Lindsay, R. Robertson, J. Shepherd, & S. Ali (Eds.), *Volcanic Atlas of the*
1100 *lesser Antilles* (pp. 65– 102). University of the French West Indies, Seismic Research Unit.
- 1101 Kranz, R. L., Harris, W. J., & Carter, N. L. (1982). Static fatigue of granite at 200 C. *Geophysical Research Letters*,
1102 9(1), 1-4.
- 1103 Le Friant, A., Boudon, G., Komorowski, J. C., Heinrich, P., & Semet, M. P. (2006). Potential flank-collapse of
1104 Soufriere Volcano, Guadeloupe, lesser Antilles? Numerical simulation and hazards. *Natural hazards*, 39,
1105 381-393.
- 1106 Legendre, Y. (2012). Reconstruction fine de l'histoire éruptive et scénarii éruptifs à la Soufrière de Guadeloupe :
1107 vers un modèle intégré de fonctionnement du volcan (Doctoral dissertation, Université Paris 7-Denis
1108 Diderot; Institut de Physique du Globe de Paris).
- 1109 Lesparre, N., Gibert, D., Marteau, J., Komorowski, J. C., Nicollin, F., & Coutant, O. (2012). Density muon
1110 radiography of La Soufriere of Guadeloupe volcano: comparison with geological, electrical resistivity and
1111 gravity data. *Geophysical Journal International*, 190(2), 1008-1019.
- 1112 Lesparre, N., Grychtol, B., Gibert, D., Komorowski, J. C., & Adler, A. (2014). Cross-section electrical resistance
1113 tomography of La Soufrière of Guadeloupe lava dome. *Geophysical Journal International*, 197(3), 1516-
1114 1526.
- 1115 López, D. L., & Williams, S. N. (1993). Catastrophic volcanic collapse: relation to hydrothermal processes.
1116 *Science*, 260(5115), 1794-1796.
- 1117 Maruvanchery, V., & Kim, E. (2019). Effects of water on rock fracture properties: Studies of mode I fracture
1118 toughness, crack propagation velocity, and consumed energy in calcite-cemented sandstone. *Geomechanics*
1119 *and Engineering*, 17(1), 57-67.
- 1120 Mastin, L. G. (1994). Explosive tephra emissions at Mount St. Helens, 1989-1991: The violent escape of magmatic
1121 gas following storms? *Geological Society of America Bulletin*, 106(2), 175-185.

- 1122 Masuda, K. (2001). Effects of water on rock strength in a brittle regime. *Journal of Structural Geology*, 23(11),
1123 1653-1657.
- 1124 Matthews, A. J., Barclay, J., Carn, S., Thompson, G., Alexander, J., Herd, R., & Williams, C. (2002). Rainfall-
1125 induced volcanic activity on Montserrat. *Geophysical Research Letters*, 29(13), 22-1.
- 1126 Matthews, A. J., & Barclay, J. (2004). A thermodynamical model for rainfall-triggered volcanic dome collapse.
1127 *Geophysical Research Letters*, 31(5).
- 1128 Matthews, A. J., Barclay, J., & Johnstone, J. E. (2009). The fast response of volcano-seismic activity to intense
1129 precipitation: triggering of primary volcanic activity by rainfall at Soufrière Hills Volcano, Montserrat.
1130 *Journal of Volcanology and Geothermal Research*, 184(3-4), 405-415.
- 1131 McBirney, A. R. (1955). Thoughts on the eruption of the Nicaraguan Volcano Las Pilas. *Bulletin Volcanologique*,
1132 17(1), 113-117.
- 1133 McGuire, W. J. (1996). Volcano instability: a review of contemporary themes. Geological Society, London,
1134 Special Publications, 110(1), 1-23.
- 1135 McKee, C. O., Wallace, D. A., Almond, R. A., & Talai, B. (1981). Fatal hydro-eruption of Karkar volcano in
1136 1979: Development of a maar-like crater. In Cooke-Ravian Volume of Volcanological Papers (Vol. 10, pp.
1137 63-84). Port Moresby, Papua New Guinea: Geological Survey of Papua New Guinea.
- 1138 Mordensky, S. P., Villeneuve, M. C., Kennedy, B. M., Heap, M. J., Gravley, D. M., Farquharson, J. I., & Reuschlé,
1139 T. (2018). Physical and mechanical property relationships of a shallow intrusion and volcanic host rock,
1140 Pinnacle Ridge, Mt. Ruapehu, New Zealand. *Journal of Volcanology and Geothermal Research*, 359, 1-20.
- 1141 Mordensky, S. P., Heap, M. J., Kennedy, B. M., Gilg, H. A., Villeneuve, M. C., Farquharson, J. I., & Gravley, D.
1142 M. (2019). Influence of alteration on the mechanical behaviour and failure mode of andesite: implications
1143 for shallow seismicity and volcano monitoring. *Bulletin of Volcanology*, 81, 1-12.
- 1144 Mordensky, S. P., Villeneuve, M. C., Kennedy, B. M., & Struthers, J. D. (2022). Hydrothermally induced edifice
1145 destabilisation: The mechanical behaviour of rock mass surrounding a shallow intrusion in andesitic lavas,
1146 Pinnacle Ridge, Ruapehu, New Zealand. *Engineering Geology*, 305, 106696.
- 1147 Moretti, R., Komorowski, J. C., Ucciani, G., Moune, S., Jessop, D., de Chabalière, J. B., ... & Chaussidon, M.
1148 (2020). The 2018 unrest phase at La Soufrière of Guadeloupe (French West Indies) andesitic volcano:
1149 Scrutiny of a failed but prodromal phreatic eruption. *Journal of Volcanology and Geothermal Research*,
1150 393, 106769.
- 1151 Moon, V., & Jayawardane, J. (2004). Geomechanical and geochemical changes during early stages of weathering
1152 of Karamu Basalt, New Zealand. *Engineering geology*, 74(1-2), 57-72.
- 1153 Moon, V., Bradshaw, J., & de Lange, W. (2009). Geomorphic development of White Island Volcano based on
1154 slope stability modelling. *Engineering geology*, 104(1-2), 16-30.
- 1155 Moune, S., Moretti, R., Burtin, A., Jessop, D. E., Didier, T., Robert, V., ... & Buscetti, M. (2022). Gas monitoring
1156 of volcanic-hydrothermal plumes in a tropical environment: the case of La Soufrière de Guadeloupe unrest
1157 volcano (Lesser Antilles). *Frontiers in Earth Science*, 10, 17.
- 1158 Nara, Y., Morimoto, K., Hiroyoshi, N., Yoneda, T., Kaneko, K., & Benson, P. M. (2012). Influence of relative
1159 humidity on fracture toughness of rock: implications for subcritical crack growth. *International Journal of*
1160 *Solids and Structures*, 49(18), 2471-2481.
- 1161 Nicolas, A., Fortin, J., Regnet, J. B., Dimanov, A., & Guéguen, Y. (2016). Brittle and semi-brittle behaviours of a
1162 carbonate rock: influence of water and temperature. *Geophysical Journal International*, 206(1), 438-456.
- 1163 Nicollin, F., Gibert, D., Beauducel, F., Boudon, G., & Komorowski, J. C. (2006). Electrical tomography of La
1164 Soufrière of Guadeloupe Volcano: Field experiments, 1D inversion and qualitative interpretation. *Earth*
1165 *and Planetary Science Letters*, 244(3-4), 709-724.
- 1166 Noël, C., Baud, P., & Violay, M. (2021). Effect of water on sandstone's fracture toughness and frictional
1167 parameters: Brittle strength constraints. *International Journal of Rock Mechanics and Mining Sciences*,
1168 147, 104916.
- 1169 Norini, G., Bustos, E., Arnosio, M., Baez, W., Zuluaga, M. C., & Roverato, M. (2020). Unusual volcanic instability
1170 and sector collapse configuration at Chimpa volcano, central Andes. *Journal of Volcanology and*
1171 *Geothermal Research*, 393, 106807.
- 1172 Opfergelt, S., Delmelle, P., Boivin, P., & Delvaux, B. (2006). The 1998 debris avalanche at Casita volcano,
1173 Nicaragua: Investigation of the role of hydrothermal smectite in promoting slope instability. *Geophysical*
1174 *Research Letters*, 33(15).
- 1175 Peruzzetto, M., Komorowski, J. C., Le Friant, A., Rosas-Carbajal, M., Mangeney, A., & Legendre, Y. (2019).
1176 Modeling of partial dome collapse of La Soufrière of Guadeloupe volcano: implications for hazard
1177 assessment and monitoring. *Scientific Reports*, 9(1), 13105.
- 1178 Pola, A., Crosta, G. B., Fusi, N., & Castellanza, R. (2014). General characterization of the mechanical behaviour
1179 of different volcanic rocks with respect to alteration. *Engineering Geology*, 169, 1-13.
- 1180 Potyondy, D. O., & Cundall, P. A. (2004). A bonded-particle model for rock. *International Journal of Rock*
1181 *Mechanics and Mining Sciences*, 41(8), 1329-1364.

- 1182 Rad, S. D., Allègre, C. J., & Louvat, P. (2007). Hidden erosion on volcanic islands. *Earth and Planetary Science*
 1183 *Letters*, 262(1-2), 109-124.
- 1184 Reid, M. E., Sisson, T. W., & Brien, D. L. (2001). Volcano collapse promoted by hydrothermal alteration and
 1185 edifice shape, Mount Rainier, Washington. *Geology*, 29(9), 779-782.
- 1186 Reid, M. E. (2004). Massive collapse of volcano edifices triggered by hydrothermal pressurization. *Geology*,
 1187 32(5), 373-376.
- 1188 Reid, M. E., Keith, T. E., Kayen, R. E., Iverson, N. R., Iverson, R. M., & Brien, D. L. (2010). Volcano collapse
 1189 promoted by progressive strength reduction: new data from Mount St. Helens. *Bulletin of volcanology*, 72,
 1190 761-766.
- 1191 Risnes, R., Madland, M. V., Hole, M., & Kwabiah, N. K. (2005). Water weakening of chalk—Mechanical effects
 1192 of water–glycol mixtures. *Journal of Petroleum Science and Engineering*, 48(1-2), 21-36.
- 1193 Rodell, M., Velicogna, I., & Famiglietti, J. S. (2009). Satellite-based estimates of groundwater depletion in India.
 1194 *Nature*, 460(7258), 999-1002.
- 1195 Rodríguez, A., & van Bergen, M. J. (2017). Superficial alteration mineralogy in active volcanic systems: An
 1196 example of Poás volcano, Costa Rica. *Journal of Volcanology and Geothermal Research*, 346, 54-80.
- 1197 Romero, J. E., Polacci, M., Watt, S., Kitamura, S., Tormey, D., Sielfeld, G., ... & Polanco, E. (2021). Volcanic
 1198 lateral collapse processes in mafic arc edifices: a review of their driving processes, types and consequences.
 1199 *Frontiers in Earth Science*, 9, 639825.
- 1200 Rosas-Carbajal, M., Komorowski, J. C., Nicollin, F., & Gibert, D. (2016). Volcano electrical tomography unveils
 1201 edifice collapse hazard linked to hydrothermal system structure and dynamics. *Scientific reports*, 6(1),
 1202 29899.
- 1203 Rosas-Carbajal, M., Jourde, K., Marteau, J., Deroussi, S., Komorowski, J. C., & Gibert, D. (2017). Three-
 1204 dimensional density structure of La Soufrière de Guadeloupe lava dome from simultaneous muon
 1205 radiographies and gravity data. *Geophysical Research Letters*, 44(13), 6743-6751.
- 1206 Rouwet, D., Tassi, F., Mora-Amador, R., Sandri, L., & Chiarini, V. (2014). Past, present and future of volcanic
 1207 lake monitoring. *Journal of volcanology and geothermal research*, 272, 78-97.
- 1208 Rutter, E. H., & Mainprice, D. H. (1978). The effect of water on stress relaxation of faulted and unfaulted
 1209 sandstone. *Rock Friction and Earthquake Prediction*, 634-654.
- 1210 Sahoo, S., Tiwari, D. K., Panda, D., & Kundu, B. (2022). Eruption cycles of Mount Etna triggered by seasonal
 1211 climatic rainfall. *Journal of Geodynamics*, 149, 101896.
- 1212 Salaün, A., Villemant, B., Gérard, M., Komorowski, J. C., & Michel, A. (2011). Hydrothermal alteration in
 1213 andesitic volcanoes: trace element redistribution in active and ancient hydrothermal systems of Guadeloupe
 1214 (Lesser Antilles). *Journal of Geochemical Exploration*, 111(3), 59-83.
- 1215 Sammis, C. G., & Ashby, M. F. (1986). The failure of brittle porous solids under compressive stress states. *Acta*
 1216 *metallurgica*, 34(3), 511-526.
- 1217 Saucedo, R., Macías, J. L., Sarocchi, D., Bursik, M., & Rupp, B. (2008). The rain-triggered Atenuique
 1218 volcanoclastic debris flow of October 16, 1955 at Nevado de Colima Volcano, Mexico. *Journal of*
 1219 *Volcanology and Geothermal Research*, 173(1-2), 69-83.
- 1220 Schaefer, L. N., Oommen, T., Corazzato, C., Tibaldi, A., Escobar-Wolf, R., & Rose, W. I. (2013). An integrated
 1221 field-numerical approach to assess slope stability hazards at volcanoes: the example of Pacaya, Guatemala.
 1222 *Bulletin of Volcanology*, 75, 1-18.
- 1223 Schaefer, L. N., Kereszturi, G., Kennedy, B. M., & Villeneuve, M. (2023). Characterizing lithological, weathering,
 1224 and hydrothermal alteration influences on volcanic rock properties via spectroscopy and laboratory testing:
 1225 a case study of Mount Ruapehu volcano, New Zealand. *Bulletin of Volcanology*, 85(8), 43.
- 1226 Scher, S., Williams-Jones, A. E., & Williams-Jones, G. (2013). Fumarolic activity, acid-sulfate alteration, and
 1227 high sulfidation epithermal precious metal mineralization in the crater of Kawah Ijen Volcano, Java,
 1228 Indonesia. *Economic Geology*, 108(5), 1099-1118.
- 1229 Schmitt, L., Forsans, T., & Santarelli, F. J. (1994). Shale testing and capillary phenomena. *International Journal*
 1230 *of Rock Mechanics and Mining Sciences & Geomechanics Abstracts*, 31, No. 5, 411-427.
- 1231 Sens-Schönfelder, C., & Wegler, U. (2006). Passive image interferometry and seasonal variations of seismic
 1232 velocities at Merapi Volcano, Indonesia. *Geophysical Research Letters*, 33(21).
- 1233 Siebert, L., Glicken, H., & Ui, T. (1987). Volcanic hazards from Bezymianny-and Bandai-type eruptions. *Bulletin*
 1234 *of Volcanology*, 49, 435-459.
- 1235 Simmons, J., Elsworth, D., & Voight, B. (2004). Instability of exogenous lava lobes during intense rainfall.
 1236 *Bulletin of volcanology*, 66, 725-734.
- 1237 Singh, T. N., Singh, S. K., Mishra, A., Singh, P. K., & Singh, V. K. (1999). Effect of acidic water on physico-
 1238 mechanical behaviour of rock. *Indian Journal of Engineering and Materials Sciences*, 6, 66-72.
- 1239 Tamburello, G., Moune, S., Allard, P., Venugopal, S., Robert, V., Rosas-Carbajal, M., ... & Moretti, R. (2019).
 1240 Spatio-temporal relationships between fumarolic activity, hydrothermal fluid circulation and geophysical

1241 signals at an arc volcano in degassing unrest: La Soufrière of Guadeloupe (French West Indies).
1242 Geosciences, 9(11), 480.

1243 Tang, S. B., Yu, C. Y., Heap, M. J., Chen, P. Z., & Ren, Y. G. (2018). The influence of water saturation on the
1244 short-and long-term mechanical behavior of red sandstone. *Rock Mechanics and Rock Engineering*, 51,
1245 2669-2687.

1246 Tanguy, J-C. (1994). The 1902-1905 eruptions of Montagne Pelée, Martinique: anatomy and retrospection. *Journal*
1247 *of Volcanology and Geothermal Research*, 60: 87-107.

1248 Taron, J., Elsworth, D., Thompson, G., & Voight, B. (2007). Mechanisms for rainfall-concurrent lava dome
1249 collapses at Soufrière Hills Volcano, 2000–2002. *Journal of volcanology and geothermal research*, 160(1-
1250 2), 195-209.

1251 Tost, M., & Cronin, S. J. (2016). Climate influence on volcano edifice stability and fluvial landscape evolution
1252 surrounding Mount Ruapehu, New Zealand. *Geomorphology*, 262, 77-90.

1253 Urlaub, M., Petersen, F., Gross, F., Bonforte, A., Puglisi, G., Guglielmino, F., ... & Kopp, H. (2018). Gravitational
1254 collapse of Mount Etna's southeastern flank. *Science Advances*, 4(10), eaat9700.

1255 van Hinsberg, V., Berlo, K., van Bergen, M., & Williams-Jones, A. (2010). Extreme alteration by hyperacidic
1256 brines at Kawah Ijen volcano, East Java, Indonesia: I. Textural and mineralogical imprint. *Journal of*
1257 *Volcanology and geothermal Research*, 198(1-2), 253-263.

1258 van Wyk de Vries, B., & Francis, P. W. (1997). Catastrophic collapse at stratovolcanoes induced by gradual
1259 volcano spreading. *Nature*, 387(6631), 387-390.

1260 van Wyk de Vries, B., Kerle, N., & Petley, D. (2000). Sector collapse forming at Casita volcano, Nicaragua.
1261 *Geology*, 28(2), 167-170.

1262 Vazquez, R., Macias, J. L., Alcalá-Reygosa, J., Arce, J. L., Jimenez-Haro, A., Fernandez, S., ... & Sanchez-Nunez,
1263 J. M. (2022). Numerical modeling and hazard implications of landslides at the Ardillas Volcanic Dome
1264 (Tacana Volcanic Complex, Mexico-Guatemala). *Natural Hazards*, 113(2), 1305-1333.

1265 Villemant, B., Hammouya, G., Michel, A., Semet, M. P., Komorowski, J. C., Boudon, G., & Cheminée, J. L.
1266 (2005). The memory of volcanic waters: shallow magma degassing revealed by halogen monitoring in
1267 thermal springs of La Soufrière volcano (Guadeloupe, Lesser Antilles). *Earth and Planetary Science Letters*,
1268 237(3-4), 710-728.

1269 Villemant B., Komorowski, J.-C., Dessert C., Michel A., Crispi O., Hammouya G., Beauducel F., De Chabaliér,
1270 (2014). Evidence for a new shallow magma intrusion at La Soufrière of Guadeloupe (Lesser Antilles).
1271 Insights from long-term geochemical monitoring of halogen-rich hydrothermal fluids. *Journal of*
1272 *Volcanology and Geothermal Research*, 285, 247-277.

1273 Violette, S., De Marsily, G., Carbonnel, J. P., Goblet, P., Ledoux, E., Tijani, S. M., & Vouille, G. (2001). Can
1274 rainfall trigger volcanic eruptions? A mechanical stress model of an active volcano: 'Piton de la Fournaise',
1275 Reunion Island. *Terra Nova*, 13(1), 18-24.

1276 Voight, B., Glicken, H., Janda, R. J. & Douglass, P. M. (1981). Catastrophic rockslide avalanche of May 18. In:
1277 Lipman, P. W. & Mullineaux, D. R. (eds) *The 1980 Eruptions of Mount St Helens*, Washington, US
1278 Geological Survey, Professional Papers, 1250, 347-378.

1279 Voight, B., Komorowski J---C., Norton, G.E., Belousov, A.B., Belousova, M., Boudon, G., Francis, P.W., Franz,
1280 W., Heinrich, P., Sparks, R.S.J. & Young, S.R. (2002) The 1997 Boxing Day Sector Collapse and Debris
1281 Avalanche, Soufriere Hills Volcano, Montserrat, W.I. In: T.H. Druitt, B.P. Kokelaar (Eds), *The eruption of*
1282 *Soufrière Hills Volcano, Montserrat, from 1995 to 1999*, Geological Society, London Memoirs, 21, 363-
1283 407.

1284 Wallace, C. S., Schaefer, L. N., & Villeneuve, M. C. (2022). Material properties and triggering mechanisms of an
1285 andesitic lava dome collapse at Shiveluch Volcano, Kamchatka, Russia, revealed using the finite element
1286 method. *Rock Mechanics and Rock Engineering*, 55(5), 2711-2728.

1287 Walter, T. R., Zorn, E. U., Harnett, C. E., Shevchenko, A. V., Belousov, A., Belousova, M., & Vassileva, M. S.
1288 (2022). Influence of conduit and topography complexity on spine extrusion at Shiveluch volcano,
1289 Kamchatka. *Communications Earth & Environment*, 3(1), 169.

1290 Wang, J. J., Zhu, J. G., Chiu, C. F., & Zhang, H. (2007). Experimental study on fracture toughness and tensile
1291 strength of a clay. *Engineering Geology*, 94(1-2), 65-75.

1292 Wasantha, P. L., & Ranjith, P. G. (2014). Water-weakening behavior of Hawkesbury sandstone in brittle regime.
1293 *Engineering Geology*, 178, 91-101.

1294 Watters, R. J., Zimbelman, D. R., Bowman, S. D., & Crowley, J. K. (2000). Rock mass strength assessment and
1295 significance to edifice stability, Mount Rainier and Mount Hood, Cascade Range volcanoes. *Pure and*
1296 *Applied Geophysics*, 157, 957-976.

1297 Wyering, L. D., Villeneuve, M. C., Wallis, I. C., Siratovich, P. A., Kennedy, B. M., Gravley, D. M., & Cant, J. L.
1298 (2014). Mechanical and physical properties of hydrothermally altered rocks, Taupo Volcanic Zone, New
1299 Zealand. *Journal of Volcanology and Geothermal Research*, 288, 76-93.

1300 Yamasato, H., Kitagawa, S., Komiya, M. (1998). Effect of rainfall on dacitic lava dome collapse at Unzen volcano,
1301 Japan. *Papers in Meteorology and Geophysics*, 48(3), 73-78.

1302 Yilmaz, T. I., Wadsworth, F. B., Gilg, H. A., Hess, K. U., Kendrick, J. E., Wallace, P. A., ... & Dingwell, D. B.
1303 (2021). Rapid alteration of fractured volcanic conduits beneath Mt Unzen. *Bulletin of Volcanology*, 83, 1-
1304 14.

1305 Young, S., Voight, B., Barclay, J., Herd, R.A., Komorowski, J-C., Miller, A.D., Sparks, R.S.J., Stewart, R.C.
1306 (2002). Hazard implications of small-scale edifice instability and sector collapse: a case history from
1307 Soufriere Hills volcano, Montserrat. In: T.H. Druitt, B.P. Kokelaar (eds), *The eruption of Soufrière Hills*
1308 *Volcano, Montserrat, from 1995 to 1999*, Geological Society, London, *Memoirs*, 21, 349-361

1309 Zimbelman, D. R. (1996). Hydrothermal alteration and its influence on volcanic hazards--Mount Rainier,
1310 Washington, a case history. University of Colorado at Boulder.

1311 Zimbelman, D. R., Rye, R. O., & Breit, G. N. (2005). Origin of secondary sulfate minerals on active andesitic
1312 stratovolcanoes. *Chemical Geology*, 215(1-4), 37-60.

1313 Zhu, W., Baud, P., & Wong, T. F. (2010). Micromechanics of cataclastic pore collapse in limestone. *Journal of*
1314 *Geophysical Research: Solid Earth*, 115(B4).

1315 Zhu, W., Baud, P., Vinciguerra, S., & Wong, T. F. (2011). Micromechanics of brittle faulting and cataclastic flow
1316 in Alban Hills tuff. *Journal of Geophysical Research: Solid Earth*, 116(B6).

1317 Zhu, W., Baud, P., Vinciguerra, S., & Wong, T. F. (2016). Micromechanics of brittle faulting and cataclastic flow
1318 in Mount Etna basalt. *Journal of Geophysical Research: Solid Earth*, 121(6), 4268-4289.